

Review

Spatially-controlled complex molecules and their applications

Yuan-Pin Chang^{a†}, Daniel A. Horke^{a†}, Sebastian Trippel^{a†} and Jochen Küpper^{a,b,c*}

^a*Center for Free-Electron Laser Science, DESY,
 Notkestrasse 85, 22607 Hamburg, Germany;*

^b*Department of Physics, Universität Hamburg,
 Luruper Chaussee 149, 22761 Hamburg, Germany*

^c*The Hamburg Center for Ultrafast Imaging, Universität Hamburg,
 Luruper Chaussee 149, 22761 Hamburg, Germany*

(July 28, 2015)

The understanding of molecular structure and function is at the very heart of the chemical and molecular sciences. Experiments that allow for the creation of structurally pure samples and the investigation of their molecular dynamics and chemical function have developed tremendously over the last few decades, although “there’s plenty of room at the bottom” for better control as well as further applications.

Here, we describe the use of inhomogeneous electric fields for the manipulation of neutral molecules in the gas-phase, i. e., for the separation of complex molecules according to size, structural isomer, and quantum state. For these complex molecules, all quantum states are strong-field seeking, requiring dynamic fields for their confinement. Current applications of these controlled samples are summarised and interesting future applications discussed.

Keywords: molecular structure; controlled molecules; quantum-state selection; conformer selection; alignment and orientation; molecular dynamics; reaction dynamics and kinetics; structure-function relationship; chirality; enantiomer separation

1. Introduction

Structure defines function. This structure-function relationship is a fundamental concept in the molecular sciences. Chemistry textbooks define structure through atomic coordinates and bond orders, using representations such as ball-and-stick models or Lewis formulas. In biology sometimes further abstractions are made, although often as additional information to the nuclear geometry: the protein data bank (PDB), for instance, typically contains coordinates of all atoms plus information on folding motifs. At the same time, we realise that it is the electrons that form and break bonds and that define the chemistry. Therefore, aren’t it the electronic wavefunctions, or the electron density, which define structure, and, thus function?

More generally, first we have to ask ourselves: Do molecules, in general, have a well-defined structure? The answer to this question strongly depends on the actual definitions of a “molecule” and a “structure”, that is, on the scientific background,

* E-mail: jochen.kuepper@cfel.de; website: <http://desy.cfel.de/cid/cmi>

† These authors contributed equally to this work.

or community, and the experiment performed. In this work, we are concerned with isolated molecules in the gas-phase. The geometric structures considered in chemistry and biology can typically be measured using spectroscopic techniques [1–5] or diffractive-imaging methods [6, 7]. We recognize that these structures depend, for instance, on the electronic state of the molecule, but still this can be disentangled spectroscopically even for large molecules [8]. Electronic structure can be experimentally observed through the (multipole) moments of the charge distribution, such as precise determinations of dipole moment vectors or polarizability tensors, possibly for individual electronic states [9, 10], but also coherent x-ray diffractive imaging measures, conceptionally, electron density.

Here, we set out to take a more specific approach to “molecular structure”, which is based on interaction properties of the molecular species, for instance, with electromagnetic fields – including these provided by other particles. Following this concept, *para* and *ortho* hydrogen (H_2) are separate species, as they exhibit very different magnetic properties and they, as isolated species, do not interconvert on typical experimental timescales. Equivalently, the structural isomers of molecules in the gas-phase typically have to be considered different molecular species, including the configurations of chiral molecules (enantiomers) or, at least in many cases, the rotational isomers of complex molecules (conformers). Chemical functionality is, for instance, intricately linked to this 3D geometric arrangement of molecules in space. This delicate structure-function relationship is especially evident in many biological systems and determines, e. g., protein folding and synthesis [11], the conformations of sugars in enzyme catalysis [12], or reactive pathways and intermediates [13]. Biology went to the extreme of homochirality and organisms use only a single configuration of all molecules involved in life [14, 15], which is a most-important structure-function relationship that still awaits a conclusive explanation. We point out that this concept of molecular structure is simply a description of the fact that, in quantum mechanics, the structure of a molecule is given by the square of the wavefunction, its probability density. In order to follow a reductionist, bottom-up description of molecular structure and function, we need to study and understand the physical and chemical properties of these individual species, how they interconvert, and how they specifically interact with their environment. This requires new experimental approaches and techniques for the preparation and investigation of the probed samples, some of which are detailed and discussed in this review.

When we prepare these molecules, or simply order them from the chemicals suppliers, we get containers containing various “molecules”, or structures, all for the price of one. A gas bottle of hydrogen contains both, *para* and *ortho* H_2 , and for glycine and tryptophan and many other complex molecules we get multiple conformers in that one bottle [16, 17]. This is due to the fact that the interconversion between structural isomers is rapid under the typical preparation and storage conditions, e. g., room temperature. Under such conditions, these species, i. e., structural isomers, are simply well connected volumes of structural phase space of these “molecules”. The molecules rapidly explore the whole phase-space volume, i. e., they change their conformation, that is, they change their “text-book structure”.

In molecular beam experiments we produce samples of cold, isolated molecules

using supersonic expansions [18, 19], where the molecules are coexpanded into high vacuum seeded in a high-pressure rare gas. In these beams the molecules are well isolated and the rare remaining collision events are very cold, i.e., have a very small energy impact [20]. The molecules still interact with the surrounding black-body radiation, but the typical timescales of the corresponding state-changing interactions are on the order of seconds [21, 22], which is much longer than the few-millisecond durations of the experiments.

1.1. Manipulating molecular species with external fields

The isolated molecules in these beams can be manipulated with external fields: Using electric fields, they can be deflected, focused, and accelerated or decelerated [22–25], they can be trapped in space [25, 26], and they can be aligned or oriented, i.e., fixed in space with respect to the directions of their dipole moments or polarizability tensors [27–30]. These methods date back to the description of polar molecules in inhomogeneous electric fields [31] and Otto Stern’s groundbreaking deflection experiments of atoms in magnetic fields [32] and of molecules in electric fields [33]; the latter already being performed in Stern’s institute for physical chemistry in Hamburg – with the original building nowadays being the historic home to our physics department. From these times, magnetic and electric fields were used interchangeably, as appropriate. Deceleration with time-varying magnetic fields has also been demonstrated during the last decade [34, 35].

Almost a century ago, Stern’s group had not only deflected molecules with electric fields and measured the electric dipole moment of potassium iodide [33]. Otto Stern also realized that there was a different regime, namely the deflection of small molecules at low temperatures, which should allow the spatial separation of quantum states [36]. Rabi developed this into the molecular beam resonance method [37]. Later, multipole focusers were used as quantum-state-specific lenses for molecules in so-called low-field-seeking states [38, 39], used in very-high-resolution spectroscopy, for instance, of ammonia [40], and to experimentally implement the MASER [41]. Similar experiments with decelerated beams of ammonia increased the achievable resolution further [42]. Many of these methods were used to study the properties of separated individual molecular species, if “only” because they created samples of molecules in a single (internal) quantum state.

The rapid and extreme cooling provided by supersonic expansions of seeded molecular beams, down below 1 K [18, 43], resulting in only few quantum states populated for polyatomic molecules, allowed to extend these techniques. More recently, over the last fifteen years, the field of ultracold molecules and cold chemistry propelled molecular physics and physical chemistry into new regimes, extensively described in a special issue on “Ultracold Molecules” in *Chemical Reviews* [44]. These reviews describe wonderful experiments and avenues into ultracold physics and chemistry, including practically fully controlled quantum-state specific reactions. However, the discussion is focused on small molecules and the issues of molecular species, such as structural isomers, is left out. This is likely due to the fact that the control of complex molecules is less advanced.

The manipulation of complex molecules with electric fields is hampered by the fact that their quantum states are all strong-field seeking under practically useful conditions. This is not of severe influence for deflection experiments, which this review focuses on. However, it makes focusing [45–49] and deceleration [50–54] cumbersome, at least. Previous overviews of such experiments are given elsewhere [22, 24, 25, 55]. Alternatively, microwave [56] and optical [57–59] ac fields were used to manipulate the motion of neutral molecules. Similarly, connected by the seminal work of Arthur Ashkin [60], very large, tens-of-nanometer- to micrometer-size “molecules” can be manipulated using radiation pressure or photophoresis *in vacuo* [61–64].

1.2. Detecting molecular species

Starting from the gas-phase-spectroscopic characterization of a second conformer of glycine [16] and the observation of multiple conformers of tryptophan even in cold supersonic expansions [65], detailed spectroscopic characterizations of these molecular species have been performed [66, 67, and references therein]. Many of these studies provide partial structural information or allow to benchmark quantum-chemistry calculations, which in turn provide structures of individual species. Moreover, these high-resolution spectroscopies allow to distinguish different species by their distinct resonance frequencies.

Alternative approaches to the investigation of the structure and dynamics of molecules are diffractive imaging techniques. Traditionally, x-ray crystallography and gas-phase electron diffraction (GED) have successfully derived structures, including those of DNA [68] and fullerene [69], respectively. Time-resolved approaches promise to allow the recording of so-called “molecular movies” of molecules *in action* [6, 70–72]. However, these techniques are not molecular species selective and, therefore, purified samples need to be provided [6, 55]. Moreover, in order to increase the obtainable information, samples of molecules fixed in space are highly beneficial and proof-of-principle experiments have been performed [73, 74].

Molecular-frame photoelectron angular distributions (MFPADs) [75] provide an alternative approach to image electronic structure. Direct photoelectrons from strong-field ionization image the electron density of the highest occupied molecular orbitals, including clear pictures of their symmetries [76–80]. Interference due to rescattering electrons results in more intricate photoelectron angular distributions, which can be considered as laser-induced electron diffraction when the wavelength of the returning electron is short [81, 82]. Alternatively, the photons generated by the coherent recombination of the accelerated electron with the ion core can be analyzed in high-harmonic-generation spectroscopy [83, 84]. Single-photon ionization can also provide a holographic electron diffraction approach to the measurements of molecular structure [85], which is applicable to complex molecules when they are strongly aligned or oriented [86, 87].

1.3. Chemistry of molecular species

The observation, understanding, and, eventually, control of quantum-state specificity of chemical reactions has been the holy grail of chemistry for a century, and it has

repeatedly been approached by different communities. Important milestones were the state-to-state reactive scattering experiments starting about fifty years ago [88], the investigation of so-called half-collisions of molecular clusters [89], and the shaped-laser-pulses coherent-control approaches [90, 91]. Successful experiments were always limited to small molecular systems, largely due to the failure to control large molecules well enough. This is combined with the difficulties to appropriately theoretically describe or model the chemistry, which is even worse for poorly defined initial conditions. Nevertheless, extremely detailed insight into chemical reactions was obtained from state-specific, cold collision studies [92, 93] as well as from ultrafast imaging experiments [7, 94].

In the remainder of this manuscript, we describe an approach to control molecules that opens new avenues for studies of the intrinsic molecular structure and dynamics of complex molecules, with the ultimate goal to develop a detailed and deep understanding of molecular function and the structure-function relationship. We give an account of the electric deflection method for the spatial separation of molecular species and quantum states and we outline the applicability of the produced controlled samples to further our understanding of these individual chemical species. In section 2 we describe the basic concepts of dc-electric-field based techniques for the manipulation of the motion and selection of individual species of neutral molecules. In section 3, we highlight selected applications in physical chemistry, and in section 4 we propose further experiments that are enabled by the current technology.

2. Background

By exploiting the Stark effect, strong electric fields provide a handle on neutral molecules, allowing for the manipulation of their motion. Here, we describe the physics of the interaction of neutral molecules with dc electric fields. Since this interaction is quantum-state specific, it allows, for instance, to spatially separate molecular beams according to quantum state. Appropriately applied, this results in the spatial separation of molecular species.

Generally these techniques are applicable to all molecules, due to the invariably non-zero polarizabilities, but for non-polar molecules the interaction strength with electric fields is typically small. Therefore, we restrict our discussion to polar molecules and to the electric-dipole-moment interaction with the electric field. Moreover, while we point out alternative techniques, we will focus our discussion on electric-field techniques and the simplest electric manipulation device, the electric deflector.

2.1. Stark effect primer

A polar molecule has a so-called permanent electric dipole moment, i.e., the centers of positive and negative electric charges are separated, in a well-defined way, in the molecular frame. This dipole's interaction with an external electric field, which results in energy shifts and wavefunction hybridization, is called the Stark effect. The resulting energy shift is given by

$$W = -\vec{\mu} \cdot \vec{\epsilon} = -\mu \epsilon \langle \cos \theta \rangle = -\mu_{\text{eff}} \epsilon \quad (1)$$

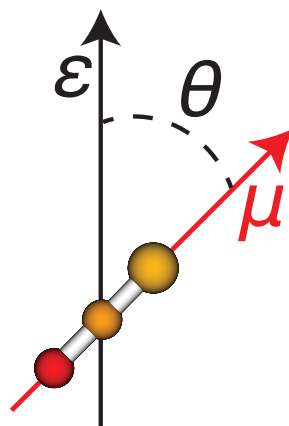


Figure 1. Electric field $\vec{\epsilon}$, electric dipole moment $\vec{\mu}$, and angle θ between them, depicted for the OCS molecule.

with the dipole moment $\vec{\mu}$ (absolute value μ), the electric field $\vec{\epsilon}$ (absolute value ϵ), and the angle θ between the two directions, as shown in Figure 1. The angular probability distribution and, therefore, the expectation value $\langle \cos \theta \rangle$ is defined by the molecule's rotational wavefunction [95]. The resulting effective dipole moment along the electric field axis is the space-fixed dipole moment $\mu_{\text{eff}} = \mu \langle \cos \theta \rangle$ of the molecule. Since $\langle \cos \theta \rangle$ is a property of the quantum state, μ_{eff} is as well.

For a molecule in field-free space the different projections M of the angular momentum onto the laboratory axis are degenerate. The angular probability density is spherical, i. e., $\langle \cos \theta \rangle = 0$ and the molecule's space-fixed dipole moment vanishes. The Stark effect lifts this degeneracy and mixes the wavefunctions, resulting in $\langle \cos \theta \rangle \neq 0$. Furthermore, the energy of the system depends on the electric field strength ϵ . Therefore, the molecule will experience a force in an inhomogeneous electric field: depending on the sign of $\langle \cos \theta \rangle$ it will be attracted towards regions of weaker or stronger electric field. Thus, providing appropriately shaped inhomogeneous electric fields enables the manipulation of the motion of molecules in space.

Theoretically, we separate the electronic and nuclear degrees of freedom through the Born-Oppenheimer approximation and the Eckart conditions [95]. For rigid closed-shell molecules in moderately strong electric fields, we can then describe the Stark interaction solely in the rotational degrees of freedom of the molecule. The rotational wavefunctions couple the molecular and laboratory frames, e. g., the (molecular-frame-fixed) dipole moment $\vec{\mu}$ and the (laboratory-frame-fixed) effective dipole moment μ_{eff} . For a polar molecule, this is described by an Hamiltonian \mathbf{H}

$$\mathbf{H} = \mathbf{H}_{\text{rot}} + \mathbf{H}_{\text{Stark}} \quad (2)$$

where \mathbf{H}_{rot} is the field-free rotor Hamiltonian and $\mathbf{H}_{\text{Stark}}$ represents the Stark interaction [95, 96]:

$$\mathbf{H}_{\text{Stark}} = -\vec{\mu} \cdot \vec{\epsilon} = -\epsilon \sum_{g=x,y,z} \phi_{Zg} \mu_g \quad (3)$$

where x, y, z represent a molecule-fixed coordinate system, μ_g represents the dipole moment components along the molecule-fixed axes x, y, z , and ϕ_{Zg} are the direction cosines of the molecular axes with reference to the space-fixed X, Y, Z -axes, with Z being oriented along the electric-field direction. Corresponding matrix elements

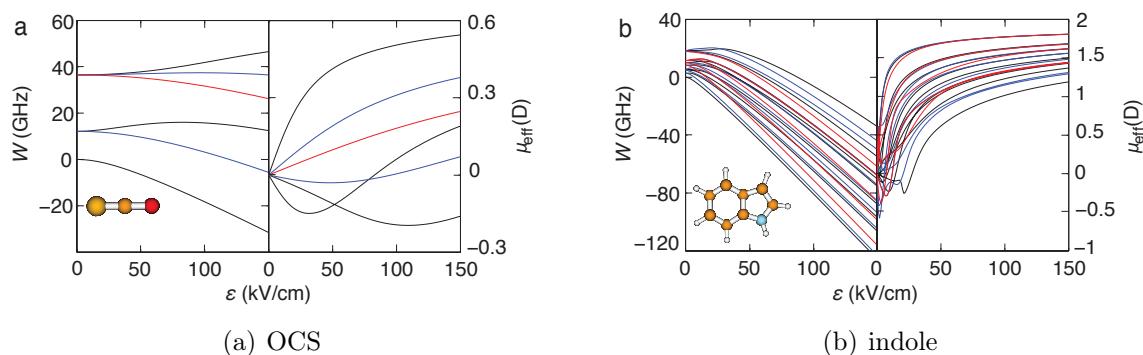


Figure 2. Stark energies W (left plots) and effective dipole moments μ_{eff} (right plots) of (a) the linear-top molecule OCS and (b) the asymmetric-top molecule indole (C_8NH_7) for the $M = 0$ (black), $M = 1$ (blue), and $M = 2$ (red) levels of all $\tilde{J} = 0\text{--}2$ states. All data were calculated using CMlStark [96]. See text for details.

to numerically set up the Hamiltonian matrix are given elsewhere [96]. Higher-order effects, e. g., the polarizability, can mostly be neglected in the case of polar molecules, although they can become relevant in very strong fields. For instance, the dipole moment ($\mu = 4.5152$ D [97]) of benzonitrile's ground state leads to an energy shift of ~ 300 GHz at 200 kV/cm, but the corresponding effect due to the polarizability of the, very similar, non-polar molecule benzene is only 50 MHz [10], i. e., almost four orders of magnitude smaller.

The energy levels of the molecule in the field, i. e., the Stark energies, are obtained by setting up the Hamiltonian matrix in the Wang-symmetrized symmetric-top basis and subsequent numerical matrix diagonalization for a number of electric field strengths. If the Hamiltonian matrix is appropriately block diagonalized exploiting the full symmetry of the problem, adiabatic Stark energy curves can simply be derived by interpolation between the appropriate calculated energies [96]. These calculations, including the appropriate symmetrization, are described in detail in reference 96, which also provides a user-friendly program to perform such numerical calculations for typical molecules. More analytical descriptions of the basic principles are given, for instance, in reference 52. The resulting Stark energy curves, depicting the quantum-state energies as a function of electric field strengths, are shown in Figure 2 for the linear molecule OCS and the asymmetric-top molecule indole. While only M remains a good quantum number in a static laboratory frame electric field, we generally add labels \tilde{J} or $\tilde{J}_{\tilde{K}_a, \tilde{K}_c}$ for the linear top OCS and the asymmetric top indole, respectively, to depict the adiabatically corresponding field-free states in order to uniquely identify the molecular quantum states, this is detailed in reference 96. Moreover, we also plot the effective dipole moment functions for the same quantum states in Figure 2, which are defined as

$$\mu_{\text{eff}}(\epsilon) = -\frac{\partial W}{\partial \epsilon} \quad (4)$$

From Figure 2a it is obvious that the Stark energies W can decrease or increase as a function of electric field strength ϵ and, correspondingly, the effective dipole moments $\mu_{\text{eff}}(\epsilon)$ can be positive or negative. Thus, depending on the quantum state, the molecules orient or anti-orient their dipole moments with respect to the electric

field and molecules in these states are attracted to regions of stronger or weaker electric field, respectively. We call these states strong-field-seeking and weak-field-seeking states, which are traditionally abbreviated as “hfs” and “lfs”, respectively.¹

As the field strength increases, so does the number of coupled J states with a significant contribution to the formed pendular states, eventually turning all low-energy states into hfs states, i. e., they start to behave like classical dipoles. Generally, the field strength at which this occurs is smaller for larger molecules, with larger moments of inertia (smaller rotational constants) and for higher-energy states, but it depends on the exact energies and coupling strengths. Moreover, avoided crossings can lead to quasi-chaotic behavior and have to be taken into account [96, 98].

The plots for OCS and indole in Figure 2 show qualitatively distinct behaviour for the plotted, and practically achievable, range of electric field strengths, highlighting the differences mentioned above. For OCS all rotational states are well separated, although the $|JM\rangle = |1,0\rangle$ state shows a turnaround from lfs to hfs state at about 83 kV/cm, which is due to the initially dominant coupling to the $|0,0\rangle$ state getting overwhelmed by the coupling to the $|2,0\rangle$ (and higher) states. Nevertheless, for these experimentally achievable field strengths the typically populated states partly show hfs and partly lfs behaviour. To the contrary, for indole these effects all occur at much smaller field strengths and under practically relevant field strengths, 50–150 kV/cm, all states are hfs. This is due to the significantly smaller rotational constants and the much larger number of states “per J ” of the asymmetric top compared to the linear top OCS. Together, these effects result in a much larger density of states, correspondingly stronger Stark mixing, and, thus, the fact that all states become hfs in relatively weak fields, i. e., $\epsilon < 25$ kV/cm, already.

2.2. Molecules in inhomogeneous electric fields

The field-strength dependence of the Stark energy, coupled with the principle of minimum energy, allows the manipulation of the motion of molecules using appropriately shaped inhomogeneous electric fields. The force \vec{F} exerted on the molecule is

$$\vec{F} = -\vec{\nabla}W = \mu_{\text{eff}}(\epsilon) \cdot \vec{\nabla}\epsilon \quad (5)$$

This force is exploited in the electric deflector to disperse a molecular beam according to the molecules’ effective dipole moments μ_{eff} , i. e., according to quantum state. An ideal electric deflection field would exert a strong and constant force in one direction, while the force in the perpendicular direction would be zero. According to Maxwell’s equations, this is not possible for hfs molecules, but one can practically approximate this case using so-called two-wire fields [99].

States with different μ_{eff} experience different deflection forces in the field, thus, traveling through the field they acquire different transverse velocities according to their dipole moment to mass ratio. Furthermore, since structural isomers of complex molecules and even molecular clusters of different sizes can have distinct dipole moments, and hence dipole moment to mass ratios, these species are transversely sep-

¹These abbreviations are used due to the originally, traditionally, used terms “high-field seeking” (hfs) and “low-field seeking” (lfs) quantum states.

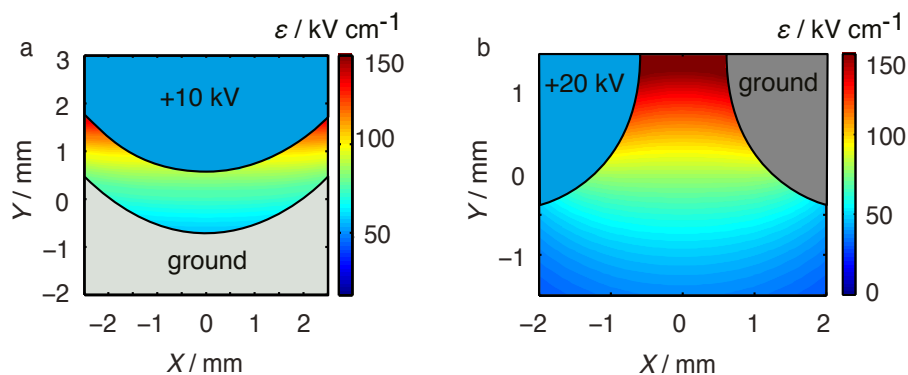


Figure 3. Two possible deflector electrode geometries: a) conventional (traditional) and b) wedge high-voltage-electrode arrangements and resulting deflection fields. The colour map indicates the magnitude of the electric field in the gap between deflector electrodes. The blue and grey areas represents the shapes of deflector electrodes, i.e., the geometric boundaries of the deflection field. The geometry on the left corresponds to the deflector and field depicted in Figure 6 and it is the geometry used in most experimental setups [99, 100, 103–107].

arated. More specifically, the species with the largest dipole moment to mass ratio is deflected the most and can cleanly be separated from all other components of the molecular beam [100]. This can be generalized to the most polar structural isomer of a complex molecule, which is deflected the most of all existing conformers and can easily be purified (see subsection 3.1).

To create inhomogeneous electric fields that provide the best forces for the manipulation of the transverse motion, a number of electric field geometries have been devised. An analysis of the electrostatic potential Φ and deflection and focusing fields $\vec{\epsilon} = -\vec{\nabla}\Phi$ can be performed in terms of a multipole expansion [52, 101, 102]. Using that formalism in two dimensions (X, Y), Φ is expressed as [102]:

$$\Phi(X, Y) = \Phi_0 \left[\sum_{n=1}^{\infty} \frac{a_n}{n} \left(\frac{r}{r_0} \right)^n \sin(n\theta) + \sum_{n=1}^{\infty} \frac{b_n}{n} \left(\frac{r}{r_0} \right)^n \cos(n\theta) \right] \quad (6)$$

using the usual cylindrical coordinates $r = \sqrt{(X^2 + Y^2)}$ and $\theta = \arctan(Y/X)$. a_n and b_n are the multipole expansion coefficients and r_0 and θ_0 are scaling factors that characterize the size of the electrode structure and the applied voltages, respectively.

Figure 3 shows two typical deflection fields, which are created by setting either all $b_n = 0$ and $|a_1| \gg |a_2| \gg |a_3| > 0$, $a_n = 0 \forall n > 3$ or, alternatively, all $a_n = 0$ and $|b_1| \gg |b_2| \gg |b_3| > 0$, $b_n = 0 \forall n > 3$. Both configurations correspond to two-wire fields [99]. They exhibit large gradients along one axis and are nearly homogeneous along the perpendicular axis. Although the resulting potentials and electric fields for the two deflector geometries are different, the magnitude of the electric field and forces at the region suitable for the molecular beam deflection are the same.

Following reference 102, the electrostatic potential and the resulting electric field

norm for the field in Figure 3 (a) can be written as

$$\Phi(X, Y) = \Phi_0 \left(a_1 \frac{Y}{r_0} + a_2 \frac{Y^2 - X^2}{2r_0^2} + a_3 \frac{Y^3 - 3YX^2}{3r_0^3} \right) \quad (7)$$

$$\epsilon(X, Y) = \sqrt{\left(\frac{\partial \Phi}{\partial X} \right)^2 + \left(\frac{\partial \Phi}{\partial Y} \right)^2} \quad (8)$$

Throughout the region $r < r_0$, we can expand the force resulting from (7) as

$$F_X(X, Y) = \mu_{\text{eff}} \epsilon_0 \left[\left(\left(\frac{a_2}{a_1} \right)^2 - 2 \frac{a_3}{a_1} \right) \frac{X}{r_0^2} - \left(\left(\frac{a_2}{a_1} \right)^3 - 4 \frac{a_2 a_3}{a_1 a_1} \right) \frac{XY}{r_0^3} + \dots \right] \quad (9)$$

$$F_Y(X, Y) = \mu_{\text{eff}} \epsilon_0 \left[\frac{a_2}{a_1} \frac{1}{r_0} + 2 \frac{a_3}{a_1} \frac{Y}{r_0^2} - \left(\frac{1}{2} \left(\frac{a_2}{a_1} \right)^3 - 2 \frac{a_2 a_3}{a_1 a_1} \right) \frac{X^2}{r_0^3} + \dots \right] \quad (10)$$

where $\epsilon_0 = (\Phi_0/r_0) \sqrt{a_1^2 + b_1^2}$. To obtain fields that are close to the ideal case described above, coefficients should be chosen such that the first term in (10) is the only significantly contributing term, while all higher-order terms, and terms in (9) should vanish. The first term in (10), the desired term, scales as a_2/a_1 while the other undesired terms scale as a_3/a_1 or as the second or third power of a_2/a_1 . We can make these undesired terms arbitrary small by choosing $a_3 = 0$ and $a_2/a_1 \ll 1$, but only at the expense of the strength of the deflection force. However, in practice one cannot afford to choose a_2/a_1 much smaller than $1/5$ [102]. The dominant undesired term in this case is the first term of Equation 9. This term can be canceled with an appropriate choice of a_3 , but this introduces other unwanted terms. Overall, for molecules in hfs states, deflection fields can provide focusing in one transverse direction, but not in both directions [52]. For example, for the deflector geometry shown in Figure 3 (a), where the value of a_3 is positive, molecules in hfs states are focused in the X direction, but they are slightly defocused in the Y direction [102]. When the value of a_3 is negative, such as the deflector geometry shown in Figure 3 (b), molecules in hfs states are focused (defocused) along the Y -axis (X -axis) instead. Typical deflectors used in actual experimental setups [99, 100, 106, 107] have geometries that correspond approximately to $a_1 = 0.5$, $a_2 = 0.49$, $a_3 = 0.42$. However, the analytical model does not describe the electric field well away from the axis ($r \neq 0$), and in practice numerically generated electric fields are used to model the experiments [100].

While focusing of hfs molecules cannot be achieved using static electric fields, alternating-gradient, so-called strong focusing, can be applied for the dynamic focusing of neutral molecules in hfs states [45, 47, 52]. Advanced concepts allow even for the deceleration of these molecules [45, 50, 51, 53, 54]. While these techniques are directly relevant for the topic discussed in this review, a detailed account is beyond the scope of this article. Extensive treatments can be found in the literature [45, 48, 52] and their use as strong-focusing storage rings has been proposed [102, 108]. Since such a storage ring could, possibly simultaneously, confine molecules in hfs and lfs states, they would offer interesting options for collision studies. However, these techniques for molecules in hfs states have not been explored much in actual applications, most likely due to their significant experimental complexity [49, 52, 53, 109]. Nevertheless,

in the following discussions of the applications of controlled molecules, we will point out results from strong-focusing manipulation where available.

2.3. State selection by deflection

Following this discussion, we can exploit the quantum-state-specific Stark effect of molecules in inhomogeneous electric fields to spatially separate molecules according to quantum state. For a given, e. g., static, electric field with an approximately spatially constant electric field gradient, such as the two-wire fields described in subsection 2.2, the force exerted on a molecule is proportional to the effective dipole moment (at the given field strength). Therefore, the deflection depends monotonically on the effective dipole moment. For a beam of molecules, which enter the deflection field all with similar speeds, this deflection field acts as a prism that disperses the molecules in the beam according to μ_{eff} , i. e., according to quantum state. Already proposed by Otto Stern in 1926 [36] for beams of small molecules at low temperatures, this technique allows the spatial separation of individual quantum states. It is also directly applicable to larger molecules, as shown here, as it always disperses the molecular beam accordingly. However, in order to create useful isolated samples, with a small subset of specific quantum states, it is of utmost importance to work with initially cold beams. These can be created, with temperatures in the moving frame reaching below 1 K, in high-pressure supersonic expansions [18, 43]. It avoids issues with non-rigidity, e. g., internal motions of the molecules [98, 110]. Correspondingly, different structural isomers are frozen and separable, as described in subsection 3.1. Moreover, the lowest-energy rotational states are the states with the smallest angular momentum, making them most suitable for orientation experiments, i. e., they have the largest effective dipole moments μ_{eff} , and thus the strongest Stark interaction. Therefore, they show the strongest response to the electric field. Since the deflection method is purely selecting molecules from the original distribution, the original number of molecules in these states, which is increased by lowering the temperature, determines the number of molecules available for an experiment with state-selected samples.

In the following, we show the results of Monte Carlo trajectory simulations of OCS molecules in a molecular beam to demonstrate state selection using electrostatic deflection fields. We also provide the source code of a prototype trajectory simulation program, with more details given in the supplementary information. In these simulations, we employ the deflection field geometry shown in Figure 3 (a), with a 15 cm long deflector, a gap between the deflector electrodes of 1.4 mm, and a radius of the rod and trough of 3.0 mm and 3.2 mm, respectively [100]. An aperture, typically a conical skimmer, is placed about 3 cm before the deflector with an orifice diameter smaller than the gap between the electrodes, e. g., 1 mm. The simulations take into account these geometric boundaries of the setup. When the molecular beam is parallel to the deflector, the mean velocities along the transverse, X and Y , axes are zero and the corresponding velocity spreads of a supersonically expanded skimmed beam are typically within a few m/s [111]. The pulsed valve is typically located some ten centimeter before the deflector. The acceleration force acting on a molecule at position (X, Y, Z) is calculated as the product of the gradient of the deflector electric field

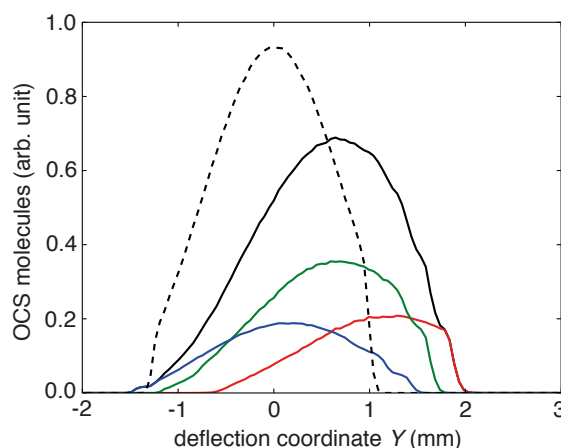


Figure 4. OCS deflection simulations of undeflected beam profile (black dash line) and with a deflection voltage of 20 kV (black solid line) at 1 K. Single state deflection profiles: $J = 0$ (red), $J = 1$ (green) and $J = 2$ (blue). See text for more details.

$\vec{\nabla}\epsilon(X, Y, Z)$ and the effective dipole moment $\mu_{\text{eff}}(\epsilon)$, which is a function of the electric field strength $\epsilon(X, Y, Z)$, see (5). For typical experimental conditions and a molecular dipole moment of a few Debye, this results in a transverse velocity component of a few m/s. This results in a deflection amplitude on the order of 1 mm after a successive free-flight distance of 20 cm. The full deflection profiles, i. e., the density distribution at some position along the beam, are calculated for individual quantum states and these profiles are added according to their populations in the incoming beam, including the Boltzmann distribution, degeneracies, and nuclear-spin-statistical weights.

Figure 4 shows the simulated deflection profiles for a beam of OCS with an initial speed of 1900 m/s, corresponding to a seeded helium expansion. The dashed black line depicts the overall profile for the undeflected beam, without any field applied, which has an identical shape for all states. Here, the gap between the deflector electrodes defines the shape and the width of the undeflected beam profile. The coloured lines are the deflection profiles of the individual rotational states $J = 0, 1, 2$, summing up all M , for an applied deflection voltage of 20 kV. The solid black line gives the weighted sum of these states for a rotational temperature of 1 K. The deflection profiles of individual rotational quantum states exhibit different shapes and deflection amplitudes due to the distinct μ_{eff} of their M levels. Particularly, the rotational ground state $|0, 0\rangle$ has the largest μ_{eff} and, therefore, experiences the largest spatial deflection. These experimental conditions allow the production of single-quantum-state samples, e. g., around the deflection coordinate $Y = 1.8$ mm, only the $J = 0$ state is present in the deflected molecular beam. Similarly, almost pure $J = 2$ state samples can be obtained below $Y = -1.2$ mm and the deflection downwards, to lower Y , is reminiscent of the lfs nature of the $|2, 0\rangle$ state at the field strengths in the deflector. Better separation could be achieved using a smaller skimmer before the deflector to provide narrower distributions for individual states. An experimental demonstration of the production of individual quantum states is described in subsection 3.3.

For the propagation of molecules in inhomogeneous (or time-varying) electric fields one has to carefully consider the adiabaticity of the process [112, 113], i. e., the assumption that molecules stay in a single well-defined adiabatic quantum state. When

the rate of change of the electric field, amplitude or direction, become too fast, non-adiabatic transitions will occur and alter the populations and the deflection profiles. Generally, when starting with a cold sample this will result in a warming of the beam, on average reducing the deflection amplitude [98]. Moreover, the complicated and dense hyperfine structure underlying the rotational-states results in complicated “partial adiabaticities”, which is due to the fact that different hyperfine levels of two rotational states might exhibit adiabatic, partially adiabatic (mesobatic), or diabatic behaviour [114, 115]. In the case of OCS, discussed here, this is not relevant as it does not have nuclear spin and thus no hyperfine splittings, and in the relevant electric field strengths the rotational states are well separated. Therefore, these molecules traverse through the experiment adiabatically. For prototypical large molecules, such as indole and 3-aminophenol (see subsection 3.1), these effects seem to be small enough to be negligible for our electric deflection experiments. In subsection 4.3 we propose some experiments to further investigate this behaviour.

We point out that the deflector, discussed here, is the simplest device in a whole series. More control can be achieved using the alternating-gradient focuser [47] and decelerator [45, 50, 52] – yielding the complete line of devices equivalent to the bender, focuser, and LINAC for charged particles, respectively. While some applications of the more complicated – theoretically and experimentally – dynamic-focusing devices are discussed in section 3, so far the deflector has made the largest impact in the manipulation of molecules in hfs states, mostly for its simplicity that allows to combine it with advanced further techniques. Moreover, the deflector has the advantage that it fully separates the manipulated molecules from the original beam. However, for higher selectivity advanced techniques need to be employed, c. f. subsection 4.4, but under these conditions dynamic focusing devices will become competitive again. A detailed discussion of these effects is beyond the scope of this paper.

The resolving power of the deflector is, as such, not well defined. Its resolution depends, for instance, on the speed of the molecules in the beam, on the size and shape of the deflector, and on the probed interaction volume, the latter being comparable to the slit of an optical spectrometer. Moreover, the achievable purity is a direct trade off with the corresponding density. The purity can also be adjusted by simply changing a skimmer-orifice size before or after the deflector. Under realistic experimental conditions, such as in the experiments described in this review, the resolution of the deflector is comparable to that of the 1-m-long dynamic focuser, for which a detailed investigation of the μ/m resolution has been carried out [48, 116].

We can estimate the experimentally achievable separation of species from the various studies carried out with the electrostatic deflector, which are summarised in section 3. Most of these experiments employed a 15 cm-long 1.5-mm-opening deflector, with typical field strengths on the order of 100 kV/cm. The interaction takes place around 20 cm behind the deflector. We note that at larger distances the achieved purity will be greater, albeit at the expense of density. The separation of individual quantum states of triatomic molecules with dipole moments on the order of 1–2 D, such as OCS [117, 118] or H₂O [119], is feasible for differences in μ_{eff} on the order of 0.1 D, which are then spatially separated by 0.1 – 0.5 mm. This is fully sufficient to address individual states with a focused laser beam. While it is even harder to pro-

vide general rules for the separation of structural isomers or clusters, we can estimate from the results presented in 3 that for molecules in the $m = 100\text{--}200$ u range, cooled to ~ 1 K, a dipole difference of 1 D is sufficient to spatially separate them by around 1 mm [110, 120, 121]. In principle, this separation can be further increased through the use of slower molecular beams, e. g., heavier backing gases, or by sacrificing target density and moving further into the tail of the deflected molecular beam distribution.

The density of molecules in the deflected beam depends on the density and velocity spread of the original molecular beam and the mechanical transmissions of skimmers and the deflector. The transmission through the deflector is only limited by its geometric size and thus only depends on the collimation and the size of the initial molecular beam, and the deflection amplitude of molecules. For the experimental setups generally used in our work, the transmission of the deflector itself is typically over 90 %, due to the application of tightly collimated molecular beams. However, when applying voltages, the spatial dispersion of molecules may significantly modify the transmission. This effect can even be used to deplete certain species from the interaction region altogether [119, 121]. In practice, using helium or neon buffer gas, and with a total distance of 80–120 cm between the molecular beam valve and the interaction region of the experiment, we achieve number densities in the deflected beam of $10^8\text{--}10^9\text{ cm}^{-3}$ [119, 120, 122].

Nevertheless, while quantitative predictions are *a priori* very difficult, we provide all tools to predict the details for any given candidate system: Our code for the calculation of Stark energy curves of linear, symmetric, and asymmetric top molecules is freely available [96], and a script to simulate trajectories of molecules through an electrostatic deflector is attached to this manuscript.

3. Applications

3.1. Conformer selection: Investigating the structure-function relationship

In order to develop a detailed understanding of the structure-function relationship, quantitative gas-phase experiments, such as measurements of absolute cross-sections or reaction rates, are essential. This requires the production of pure samples of individual conformers, that is, the ability to separate molecular species with distinct structures, c. f. section 1. For charged systems this has been demonstrated using ion-mobility schemes [123–126] or spectroscopic methods such as selective ionisation of neutral precursors [127, 128]. While the former is not applicable to neutral molecules, several spectroscopic schemes have been used for the production of conformerically pure (or enriched) samples of neutral molecules in the gas-phase, e. g., stimulated-emission pumping [129] or IR-induced population transfer [130]. However, these spectroscopic methods are not generally applicable for the separation of arbitrary neutral conformers and, furthermore, do not spatially separate these. Thus, they do not allow non-species-specific investigations, such as strong-field ionisation or diffractive imaging. These shortcomings are addressed by the separation techniques using strong inhomogeneous electric fields. The first demonstration of conformer separation by strong fields used alternating gradient focusers, through which, for a given ac frequency, only molecules with selected m/μ_{eff} ratios have stable trajectories [47, 48].

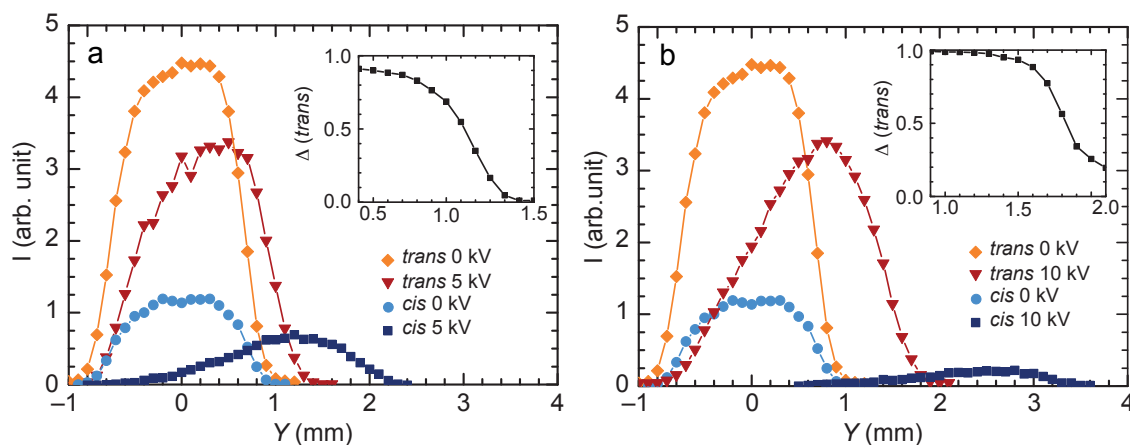


Figure 5. Separation of structural isomers of 3-aminophenol (3AP) with the electrostatic deflector. a) Due to its larger μ_{eff} the *cis* isomer experiences a larger deflection and pure samples can be obtained in a Neon beam at deflection voltages of 5 kV. b) Higher voltages, of 10 kV, can be used to remove all *cis* population from the molecular beam, leaving a pure *trans* sample. The insets show the fractional population Δ of *trans*-3AP in the beams; see text for details.

This approach is, however, technologically extremely challenging. The switching of large voltages (tens of kV) at kHz repetition rates is demanding, and the necessary (multiple meter) long quadrupole electrodes are extremely sensitive to mechanical misalignment [52, 109, 131]. An experimentally much simpler device is the electrostatic deflector, which can be designed to produce a simple two-wire field, as outlined in subsection 2.2 [99]. It is generally applicable to all neutral molecules, including hfs states and even very large systems, and, similar to alternating-gradient systems, spatially separates species on the basis of m/μ_{eff} ratio, but provides no radial focusing.

The selection of different conformers in the deflector is based on their differing dipole moments due to a different arrangement of the functional groups in space. This has been demonstrated for several small aromatic systems exhibiting two conformers [120, 121, 132]. An example of the achieved separations and resulting conformeric purities is shown in Figure 5 for the separation of *cis*- and *trans*-3-aminophenol (3AP) [120]. Here, pure samples of both conformers can be produced and the species of interest selected *via* the applied deflector voltage. Using a Neon expansion, 5 kV is sufficient to separate the more polar *cis* conformer from the rest of the beam and obtain isolated samples, Figure 5 a. The obtained pure sample contains only the lowest energy quantum-states, as these experience the largest deflection in the electric field, c.f. subsection 2.1. In order to also produce pure samples of the less polar conformer, in this case *trans* 3AP, the voltage applied to the deflector is increased further to 10 kV. At these voltages the *cis* isomer is deflected so much the it does not reach the interaction region anymore, Figure 5 b. A sample containing only the lowest rotational quantum-state of *trans* is now produced in the region of $Y = 1.4$ mm. A similar conformer separation and production of rotationally cold samples has also been demonstrated for 3-fluorophenol recently [121]. This method is generally applicable to systems with two populated conformers that differ in their dipole moment. The produced pure and cold samples, which for smaller molecules can even be single quantum-states as shown in subsection 3.3, are beneficial in a variety of further experiments, such as molecular alignment and orientation control [30, 100, 118, 133].

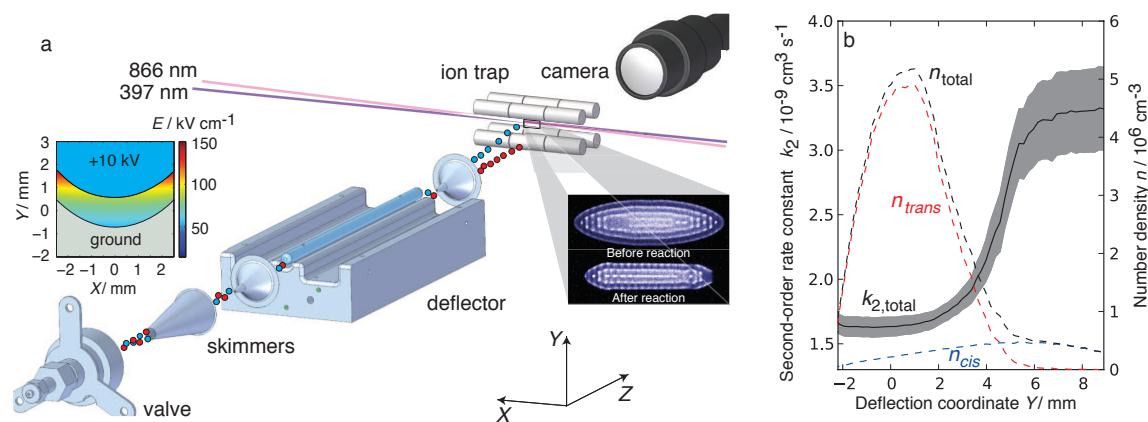


Figure 6. Conformer-selected chemistry investigated through reactive collisions between *trans* and *cis* 3-aminophenol with laser-cooled Ca^+ ions in a Coulomb crystal. (a) Experimental setup combining the electrostatic deflector with the quadrupole ion trap containing the Coulomb crystal. Tilting of the molecular beam relative to the trap allows to select the conformer incident on the crystal. (b) Measured second-order rate constant as a function of deflection coordinate. Shown as dashed lines are the relative intensities for each conformer at that position. Reproduced from reference 122. Reprinted with permission from AAAS.

Recently, the conformer separation with static electric fields has been used to study conformer resolved reactions in scattering experiments of conformationally selected neutral molecules with trapped cold atomic ions [122, 134]. Specifically, conformer-selected molecular beams of *cis*- and *trans*-3-aminophenol were collided with a stationary target of laser-cooled Ca^+ ions and the reaction rate measured for both conformers, this experimental setup is shown in Figure 6a. By measuring the rate constants at different points in the deflected molecular beam, shown in Figure 6b, the conformer-specific rate constants were extracted and the *cis* conformer found to have a rate constant approximately twice that of the *trans* species. Measurement of the number densities in the molecular beam furthermore allowed the extraction of absolute values for the second order rate constant for each conformer. These findings were explained with conformer-specific differences in the long range interaction potential of the molecule and ion, stemming from the conformation-dependent electrostatic properties of the molecules. This experiment nicely demonstrates the fact that these conformers exhibit distinct chemical properties, i.e., are separate molecular species as outlined in section 1.

This proof-of-principle experiment shows the detailed level of quantitative information to be gained from conformer-resolved gas-phase experiments, and several extensions to this setup are currently being planned or implemented. The production of molecular Coulomb crystals [135], sympathetically-cooled from collisions with laser-cooled atoms, opens up possibilities for the study of ion-molecule reactions, with the possibility to extract absolute densities and rate constants for individual conformer reactions. These experiments can add further selectivity by employing narrowband resonant ionisation schemes for the production of ions, yielding rotational and vibrational state specificity for the ionic reaction partner [136].

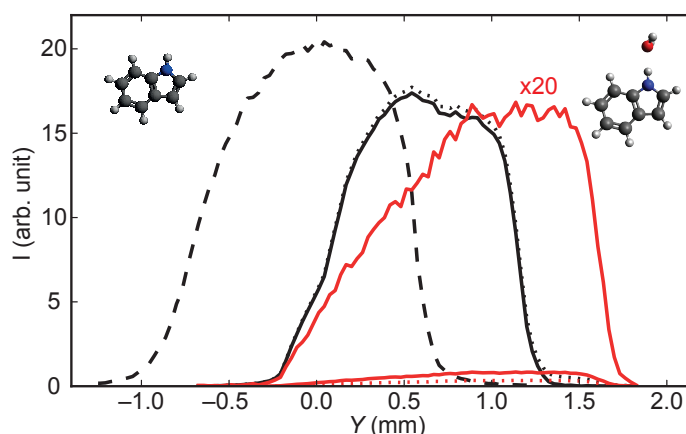


Figure 7. Deflection profiles from the co-expansion of indole and water, leading to the formation of indole(H_2O) $_n$ clusters. The dashed line shows the field-free molecular beam profile. Dotted lines indicate measured signal at the mass channels corresponding to singly charged bare indole (black) and indole(H_2O) (red). Solid lines show the molecular beam density, corrected for fragmentation of the indole(H_2O) cluster. At vertical positions in the range ~ 1.4 – 1.8 mm a pure indole(H_2O) cluster beam is obtained.

3.2. Cluster selection: From gas-phase to bulk chemistry

There is substantial interest in the study of molecular cluster systems, which could bridge the gap between the gas-phase, where highly detailed investigations of the intrinsic molecular properties are feasible, and the condensed phase, where the majority of chemistry occurs. Furthermore, clusters allow to sequentially and systematically add solvent molecules to the molecular species of interest. This aids approaches to unravel the effects of solvation, for instance, on electronic structure. Significant literature is available on the study of ionic clusters, where size-selection is trivial using mass-spectroscopic techniques [137, 138]. This is not the case for neutral cluster experiments, where experimenters have so far primarily relied on the spectroscopic identification of formed clusters, and only few experimental techniques can physically separate clusters, such as scattering from a secondary Helium beam [139–141]. The application of the alternating-gradient focuser to the separation of cluster systems has recently been demonstrated in a proof-of-principle experiment. Here, benzonitrile-argon clusters could be separated partially from benzonitrile due to the different masses, but nearly identical dipole moments, of the complexes [142]. Use of the simple electrostatic deflector offers a widely applicable method of producing pure clusters beams. It relies on different cluster stoichiometries possessing differing dipole moments and/or different masses, too, allowing their separation according to the m/μ_{eff} ratio. In molecular beam experiments this enables the separation of small clusters from remaining monomers or other cluster stoichiometries in the beam. Furthermore, this method is in principle also sensitive to the geometric structure of the cluster through the dipole moment dependence and should enable the separation of different structural cluster isomers, e.g., the different geometries of the water hexamer [5].

While it is not *a priori* clear if the deflection technique is applicable to larger, floppy molecular systems such as clusters, containing such high densities of states and correspondingly complex Stark energy curves with multiple avoided and real

crossings, its applicability to small cluster systems has recently been demonstrated in the study of indole(H_2O) $_n$ clusters [110]. Here, indole and water were co-expanded in a helium-seeded molecular beam, leading to the formation of a *cluster soup*, containing the respective monomers and different clusters of the type indole(H_2O) $_n$. The produced beam was directed into a 15 cm long deflector with field strengths on the order 120 kV/cm. Spatial profiles were recorded species-selectively for indole and water monomers as well as the indole(H_2O) clusters using resonance-enhanced multiphoton ionization (REMPI) [110]. While in the absence of a deflection field all species are spatially overlapped, application of strong fields broadens the observed distributions, due to the different μ_{eff} of occupied rotational states. The indole(H_2O) cluster possess the largest dipole moment ($\mu = 4.4$ D) [143] and is deflected significantly more than indole ($\mu = 1.96$ D). Similarly, water molecules ($\mu = 1.86$ D) and higher order clusters such as indole(H_2O) $_2$ ($\mu = 2.63$ D) are deflected significantly less [110]. Figure 7 shows an updated experiment of the cluster separation with a colder beam than in the original experiment. Here, strong-field ionization mass-spectrometry was used in a high-repetition-rate experiment [106]. This leads to the production of a pure indole(H_2O) sample, at spatial positions $1.4 < Y < 1.8$ mm. The spatial dispersion of rotational quantum states furthermore means that at the edge of the deflected profile only the lowest ~ 290 rotational quantum states of indole(H_2O) are present, compared to ~ 4600 states in the original beam [110]. An electrostatic deflector, therefore, not only produces a pure cluster beam, but also yields lower effective rotational temperatures than can be obtained from supersonic expansion alone.

3.3. Separation of individual quantum states

The production of single quantum states samples is a routine technique for low-field-seeking (lfs) states in small molecules, first developed in the 1950s [39, 144] and relying on multipole focusers and static fields to guide and select lfs quantum states [25, 145–147]. These were crucial for the development of the first MASER [38, 41], and later on in the first inelastic and reactive state-specific scattering experiments [148–150]. The inability to create a field maximum in free space, however, restricts these methodologies to lfs states, and, therefore, cannot produce isolated ground state samples of larger molecules, for which all low-lying quantum states are hfs. The Stark deflection technique presented here does allow the separation of hfs quantum-states through the quantum-state dependence of the effective dipole moment μ_{eff} . It does, however, not provide guiding or focusing of the selected molecules, meaning that devices are typically restricted to shorter lengths to ensure sufficient densities in the interaction region. Dynamic field techniques, such as alternating-gradient focusers [49], have demonstrated the ability to provide guiding for state-selected hfs states, albeit at the expense of experimental simplicity, making it extremely challenging to incorporate these devices into existing experimental setups. To achieve a full separation of quantum-states with the Stark deflector, the difference in μ_{eff} for neighbouring states must be sufficiently large to separate them. This is the case for small molecules with correspondingly large rotational constants and rotational energy level separation. Specifically, single-quantum states of OCS [117, 118] and water [119] have been pro-

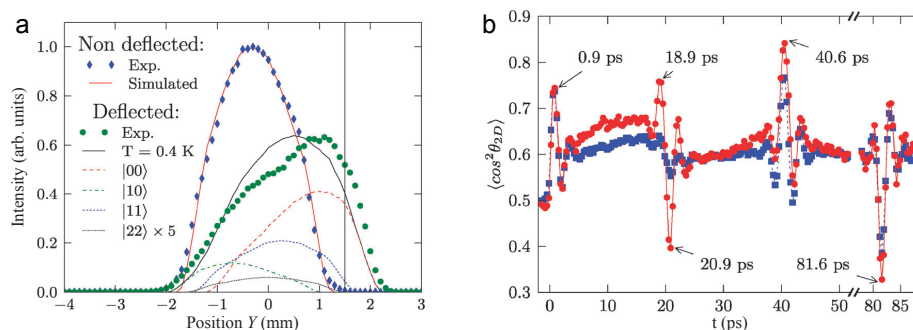


Figure 8. Quantum-state separation of OCS. (a) Molecular beam intensity profiles (data points) and simulations for individual quantum states (dashed lines) and for a convolution at 0.4 K rotational temperature (solid line). (b) Non-adiabatic alignment dynamics for OCS, as characterised by the time-dependent degree of alignment $\langle \cos^2 \theta_{2D} \rangle$, for the direct beam (blue) or the deflected beam at 1.5 mm (red). Reproduced from reference 117 with permission of The Royal Society of Chemistry.

duced in the gas-phase. As electrostatic deflection does not change the population of quantum-states in the molecular beam, but rather disperses it, a large initial population of the lowest quantum states, i.e., a low rotational temperature, is crucial to these experiments.

The first demonstration of single-quantum states produced with the electrostatic deflector was for OCS molecules [117]. OCS was produced *via* supersonic expansion in a pulsed valve, producing a molecular beam in the electronic and vibrational ground state ($X^1\Sigma^+ |00^0 0\rangle$) and with a rotational temperature < 1 K. The beam is then dispersed by a 15 cm long electrostatic deflector, leading to a spatial separation of rotational quantum states due to their different effective dipole moments. This is shown in Figure 8a, along with corresponding trajectory simulations indicating the contributions of different quantum states and the overall ensemble temperature, introduced in subsection 2.3 [96]. This experiment did not employ quantum-state resolved detection, but the separation of quantum states could directly be inferred from comparison to theory as well as a variant of rotational-coherence spectroscopy. The comparison with the trajectory simulations indicate that at the position $Y = 1.5$ mm at least 85% of molecules are in the absolute ground state $|00\rangle$. An impulsive-alignment experiment shows clear quarter-revival features for the deflected beam, Figure 8b, which are the direct result of an ensemble of defined parity. Comparison of the phase and amplitude of the revivals with quantum-dynamics calculations indicate a purity of 92% of the $|00\rangle$ state in the deflected beam [117].

The production of single-quantum-state samples of large molecules in hfs states has also been demonstrated using alternating-gradient focusing [49]. These setups allow one to tune the transmitted μ_{eff}/m range by changing the electrode switching frequency and voltages. This allowed the production of pure absolute ground state samples of benzonitrile and a $\mu/\Delta\mu$ resolution ~ 20 is achieved [49]. The application of the deflector for the production of single-quantum-state samples of small asymmetric top molecules was recently demonstrated with the first full separation of the nuclear spin states, *para* and *ortho*, of water [119]. Here, the two absolute ground states of the nuclear-spin isomers could be spatially separated and pure samples of either obtained. These isomers differ only in the relative orientation of the hydrogen

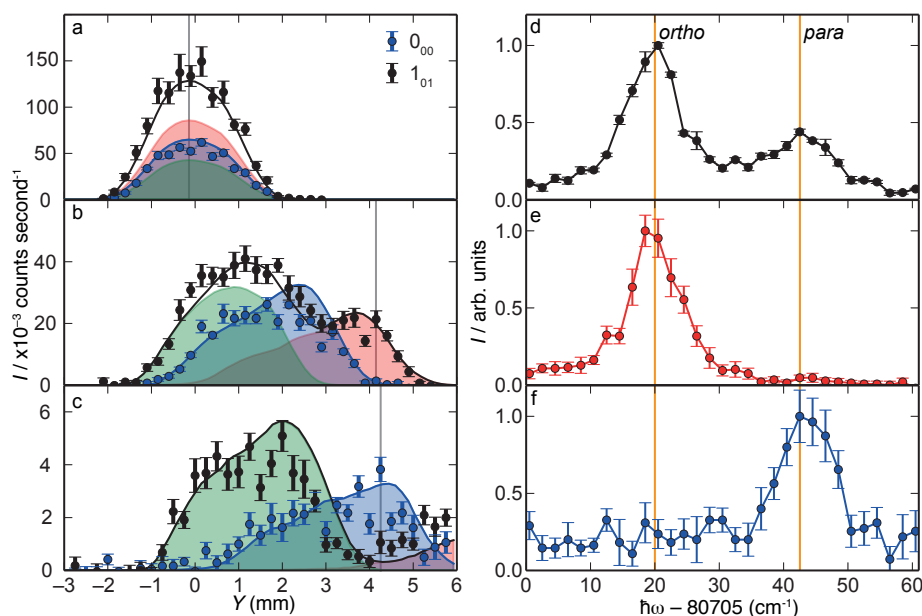


Figure 9. Separation of the nuclear-spin isomers of water with the electrostatic deflector. On the left are spatial profiles measured using REMPI (data points) and the corresponding simulations (solid lines), the shading indicates the $|0_{00}\rangle$ (green), $|1_{01}0\rangle$ (blue) and $|1_{01}1\rangle$ (red) states. Profiles are shown for a Neon expansion at (a) 0 kV and (b) 15 kV, and for Argon at 15 kV (c). Corresponding REMPI spectra are shown in d-f, recorded at the position marked by the grey lines in the spatial profile.

nuclear spins, leading to a symmetric (*para*) and an antisymmetric (*ortho*) spin wavefunction. The symmetrization postulate of quantum mechanics requires the overall molecular wavefunction to be antisymmetric, and, therefore, the nuclear spin states reside in different rotational states. A cold water beam was produced in a supersonic expansion, leading to rotational temperatures < 7 K, but nuclear-spin populations that are frozen at the room-temperature limit of 1:3 *para*- to *ortho*-water. The absolute ground states $|J_{K_a K_c}\rangle$ of these two species are $|0_{00}\rangle$ for *para*- and $|1_{01}\rangle$ for *ortho*-water, respectively. In the presence of an electric field the M degeneracy will be lifted, splitting the *ortho*-water state into $M = 0$ and $M = \pm 1$ components, with distinctive μ_{eff} . These three populated states can all be separated with the electrostatic deflector, as shown in Figure 9 [119]. The $|1_{01}1\rangle$ has the largest μ_{eff} and, therefore, undergoes the largest deflection; this can be separated from all other quantum-states, Figure 9 b and e. To produce pure *para*-water the deflection is increased through the use of a heavier backing gas and, therefore, slower molecular beam, which increases the interaction time with the electric field. This deflects all $|1_{01}1\rangle$ population out of the interaction region and produces a pure $|0_{00}\rangle$ sample, Figure 9 c and f. A sample of $|1_{01}0\rangle$ can be accessed with this configuration at the undeflected beam position, as all other quantum states have been deflected away. These separated nuclear-spin isomers of water could allow significant applications in astrophysics and -chemistry as well as novel NMR imaging techniques. Furthermore, it highlights the general applicability of the deflector to access the absolute ground state of neutral molecules, due to its sensitivity to hfs species. Moreover, it adds further support for the concept of molecular structure and species brought forward in section 1.

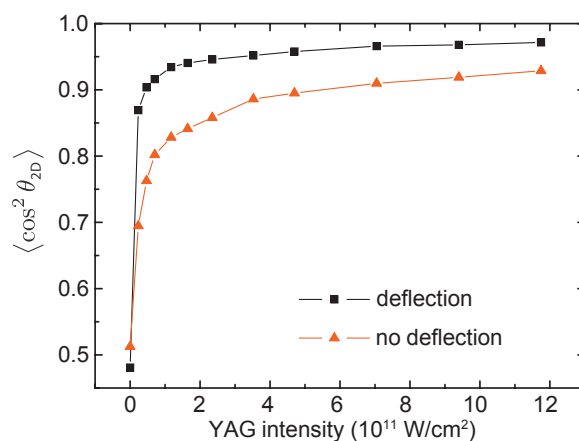


Figure 10. Degree of alignment observed for iodobenzene molecules for different alignment laser intensities, recorded with a direct molecular beam (red) and with the coldest part from an electrostatically dispersed beam (black). Reprinted with permission from reference 100. Copyright 2009, AIP Publishing LLC.

3.4. Cold molecular samples through rotational-state dispersion

The selection of a single rotational quantum state of a molecule gets increasingly harder as the molecular structure gets larger and, therefore, the density of states increases. However, the electrostatic deflection technique, nonetheless, leads to a dispersion of the rotational states by their effective dipole moment, equivalent to the dispersion of white light by a prism. As the lower rotational states have larger μ_{eff} , Figure 2, these are deflected the most, leading to a spatially dispersed rotational state distribution. This is not an active cooling process as the population distribution among the rotational states remains unchanged, but rather allows the probing of a lower effective rotational temperature by excluding high J states from the probe volume. Therefore, this technique will reduce the number density available and requires a high initial population of the lowest rotational states, necessitating a cold initial molecular beam.

One important application for these internally-ultra-cold samples are molecular alignment and orientation experiments [151]. Especially in the regime of long-pulse “adiabatic” alignment [29, 106, 118], these experiments benefit from the lower- J state distribution in the deflected part of the molecular beam and a higher degree of alignment can be reached, as shown in Figure 10 [30, 100]. This has been demonstrated for several small aromatic molecules [30, 77, 152] and, furthermore, has been extended to kilohertz repetition rates [106]. When combined with the single-quantum-state selection achieved for OCS, this allows for the observation and exploitation of specific quantum-mechanical effects. For example, Raman-type couplings during the switch-on of a strong laser field lead to the creation of a pendular-state wavepacket, forming a strongly driven quantum-pendulum, observable through the degree of molecular alignment [118]. A similar effect of coherent superposition of states within strong fields can be utilized to achieve field-free orientation of molecules, as the coherent superposition persists, and, therefore, revives, even after the laser pulse has been turned off [133].

3.5. Imaging experiments using novel light sources

The advance of new coherent x-ray light sources providing ultrashort pulses, such as free-electron lasers and high-harmonic generation techniques, offer the opportunity to record nuclear dynamics at the ultrashort timescales at which atomic motion occurs, allowing the recording of *molecular movies*. Such sources are, however, highly reliant on the controlled and reproducible delivery of samples into the interaction region. For x-ray diffraction techniques on isolated molecules, it is furthermore highly desirable to control the spatial alignment and orientation of molecules. A further complication when studying gas-phase species with ionizing radiation is the typically low number density of molecules, especially when compared to the carrier gas of the molecular expansion, which is on the order of 10^4 as dense.

Several of these experimental difficulties can be addressed using the electrostatic deflection technique. As outlined above, the dispersion of rotational quantum-states allows the production of colder ensembles of molecules, which can be used to achieve unprecedented degrees of alignment. Furthermore, as the monoatomic carrier gas passes through the deflector unaffected, the molecules of interest are actually separated from the stream of backing gas, potentially significantly reducing the background signal observed in X-ray experiments, such as single molecule diffractive imaging [74] or photoelectron diffraction in aligned molecules following core-shell excitation with x-ray pulses [87, 153]. Finally, as these x-ray experiments are inherently non species-selective, a pure sample in the interaction region is required. Using the electrostatic species separation, this is now feasible for large complex molecules containing several conformers, and even weakly-bound cluster systems.

A recent proof-of-principle experiment has demonstrated this approach with the first x-ray-diffraction measurement from aligned gas-phase molecules using a free-electron laser [74, 154]. These experiments can provide direct access to structural information. 2,5-diiodobenzonitrile molecules were supersonically expanded into vacuum and subsequently dispersed by the electrostatic deflector to select a colder sample. These molecules were adiabatically aligned with a nanosecond laser pulse and irradiated with bright x-ray pulses from the Linac Coherent Light Source, whose direct scattering was recorded. A typical experimental setup is shown in Figure 11 a. The alignment laser and x-ray pulses are combined using a holey mirror and propagate collinearly, crossing the state-selected molecular beam at right angles. The interaction takes place within a velocity-map imaging spectrometer, where ion imaging is utilized to quantify the degree of alignment of the target molecules. Scattered x-rays are recorded on a pnCCD detector, with a central gap to let the main beams pass through. Recorded and simulated difference diffraction patterns of aligned and randomly oriented molecules are shown in Figure 11 b, along with the corresponding angular distribution histograms. In this proof-of-principle experiment the dominant scatterer are the heavy iodine atoms, and the recorded diffraction images allowed the authors to infer the iodine-iodine distance in 2,5-diiodobenzonitrile, in good agreement with literature and simulated values. These results demonstrate the feasibility of measuring structural information from diffraction images of single molecules, aligned in the gas-phase. The very strong degree of alignment is essential in experiments aimed at extracting molecular frame 3D structural data, and it is the electrostatic

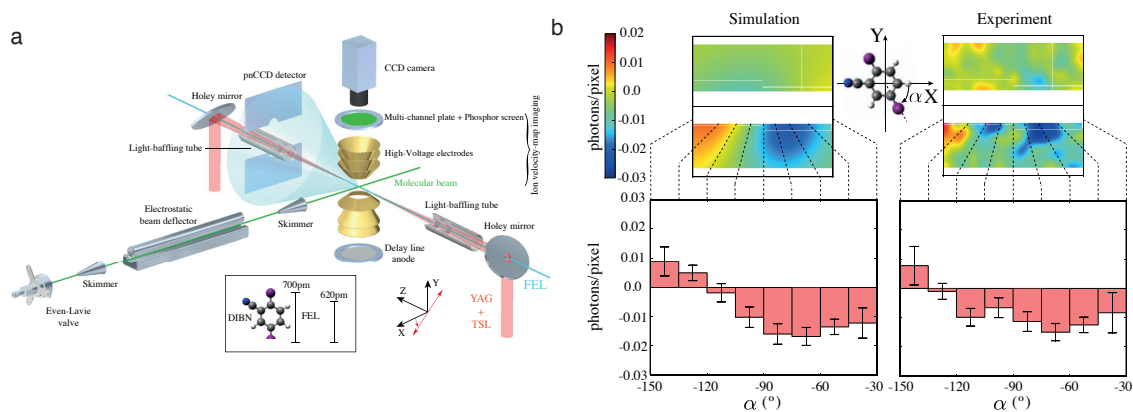


Figure 11. X-ray diffraction from aligned molecules. (a) Experimental setup with high-pressure valve and electrostatic deflector for the production of ultracold molecular samples. The interaction takes place inside a VMI spectrometer to monitor the degree of alignment using ion imaging. X-ray diffraction patterns are recorded on a pnCCD detector. (b) Simulated and experimental difference diffraction patterns and angular histograms for diffraction of 2 keV photons from 2,5-diiodobenzonitrile. Reprinted with permission from reference 74. Copyright 2014 by the American Physical Society.

deflection technique that provides the necessary ultracold molecular samples for this.

4. Outlook

4.1. Separation of very large molecules

A variety of new and exciting applications can be envisioned for the electrostatic deflector. The separation of conformers and quantum states holds in general. In practice, it allows the separation of molecular species that differ sufficiently with respect to their effective dipole moments in strong electric fields. The influence of very strong electric fields on both the orientation of the dipole as well as structural changes have been investigated theoretically for large molecules such as polyanilines [155] or the enzyme lysozyme [156]. Our simulations show that the molecular dipole moment becomes oriented in static electric fields for field strengths on the order of 100 kV/cm. Structural transformations that distort the molecular structure only appear at significantly higher field strengths [155, 156] and these effects do not play a significant role for the experimental conditions in the deflector. Thus, the dispersion of beams of such molecules is feasible and will allow for a, at least partial, separation of different species. Especially for the helical structures of peptides, in which all amino-acid dipoles are parallel, a very strong deflection and the separation from other folding motifs can be expected.

4.2. Separating the enantiomers of chiral molecules

Preparing molecules in a certain quantum state could be beneficial for precision experiments to test fundamental physics. The CPT theorem states that the laws of physics are invariant under the simultaneous transformations of charge conjugation (C), parity transformation (P), and time reversal (T). Although CPT is conserved, parity (P) might not be conserved in processes involving the weak force [157, 158]. This leads to parity-violation effects, e.g., between the two enantiomers of chiral

molecules [159, 160].

The potential energy surface of a chiral molecule shows two minima separated by a barrier. These minima may be associated with the left ‘L’ and right ‘R’ enantiomers. When the interconversion barrier is high, the right and left state can be, to a good approximation, considered as energy eigenstates. These eigenstates are degenerate within quantum mechanics in the absence of the weak force. In the presence of the weak force however, a small parity violation energy difference is expected between the ground states and excited states of the enantiomers. Therefore, right- and left-handed molecules are not exact mirror images of each other. The energy differences of enantiomers is predicted in the femtojoule to picojoule per mole range [161]. This small difference is the reason why parity violation effects in chiral molecules have so far never been observed experimentally. The energy differences between two enantiomers might be accessible in high-resolution laser- or microwave-spectroscopy [159, 162, 163]. In order to study parity violation effects in molecules it would be highly beneficial to study both enantiomers individually in order to determine the differences in the energy eigenstates. The electrostatic deflector might provide a useful tool in order to separate both enantiomers, online, for future high precision experiments as well as for further investigations of their individual properties, including chemical reactions [122].

For such an experiment, one could, for instance, start with two enantiomers of a molecule in the absolute ground state. This would be achieved, for a molecule such as CHBrClF , with the smallest rotational constant on the order of 1 GHz, at a rotational temperature of about 10 mK or using an appropriate state-selection experiment (see, e.g., subsection 3.3). Starting from both enantiomers in their ground state, one could, using resonant microwaves, prepare one of the enantiomers in a rotationally excited state before it enters the deflector, while the second enantiomer stays in its ground state. The two enantiomers will then be deflected differently due to the different space-fixed dipole moments μ_{eff} of the two states. The method to excite only one enantiomer is conceptionally similar to the enantiomer-specific detection of chiral molecules by microwave spectroscopy [164].

Asymmetric top molecules have three inequivalent principal axes of inertia, a, b, c , with rotational constants A, B , and C , which describe the rotational energy levels. The corresponding magnitudes of the dipole moment components, $|\mu_a|, |\mu_b|, |\mu_c|$, determine the strengths of transition between the rotational energy levels of such a molecule, while the sign of $\mu_a \cdot \mu_b \cdot \mu_c$ is directly connected to its chirality. For simplicity, both enantiomers are assumed to be in their absolute ground state $|g\rangle$ initially. The two enantiomers are exposed to a resonant $\pi/2$ pulse with polarization, for instance, along the a axis, i.e., corresponding to an a -type transition. This creates a superposition state, $|1\rangle = 1/\sqrt{2}|g\rangle + 1/\sqrt{2}|e_a\rangle$, between the ground $|g\rangle$ and some excited state $|e_a\rangle$ as indicated in Figure 12 a by the red quarter circle and arrow.

A second $\pi/2$ laser pulse with a polarization perpendicular to a , e.g., b , which is resonant to a b -type transition, mixes in components of a second excited state $|e_c\rangle$ with complex phases proportional to μ_b (purple and blue lines). The phase between the applied a -type transition that mixes $|g\rangle$ and $|e_a\rangle$ and the b -type transition that mixes $|e_a\rangle$ and $|e_c\rangle$, has to be ideally chosen such that the new state $|2\rangle$ is given by

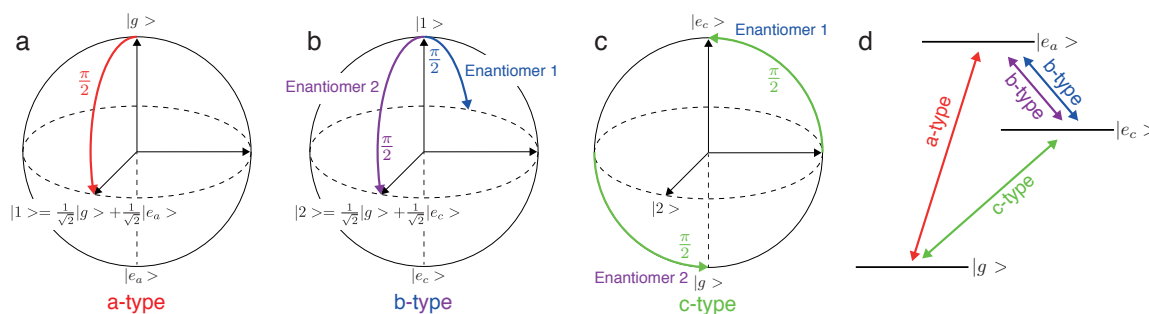


Figure 12. Illustration of the excitation scheme to transfer one enantiomer to the excited state. a) Bloch-sphere of the two-level system consisting of the states $|g\rangle$ and $|e_a\rangle$. The $\pi/2$ pulse of the corresponding *a*-type transition, that transforms both enantiomers to the pure state $|1\rangle = 1/\sqrt{2}|g\rangle + 1/\sqrt{2}|e_a\rangle$, is indicated by the red quarter circle. b) Bloch-sphere of the two-level system consisting of the states $|1\rangle$ and $|e_c\rangle$. The $\pi/2$ pulse of the corresponding *b*-type transitions is indicated by the blue quarter circle for enantiomer 1 and the purple quarter circle for enantiomer 2. The phase between the applied *a*- and *b*-type transitions has to be such, that the resulting state $|2\rangle = 1/\sqrt{2}|g\rangle + 1/\sqrt{2}|e_c\rangle$ has no contribution from $|e_a\rangle$. c) Bloch-sphere of the two-level system consisting of the states $|g\rangle$ and $|e_c\rangle$. The $\pi/2$ pulse of the corresponding *c*-type transition, that transfers the system from the state $|2\rangle$ to the excited state $|e_c\rangle$ for enantiomer 1 and to the ground state $|g\rangle$ for enantiomer 2, is indicated by the green quarter circles. d) Level diagram of the involved states and transitions.

$|2\rangle = (1/\sqrt{2}|g\rangle + 1/\sqrt{2}|e_a\rangle) - (1/\sqrt{2}|e_a\rangle - 1/\sqrt{2}|e_c\rangle) = 1/\sqrt{2}|g\rangle + 1/\sqrt{2}|e_c\rangle$. The resulting state $|2\rangle$ has no contribution from $|e_a\rangle$ and the two pulses have now created a superposition of the two states $|g\rangle$ and $|e_c\rangle$ oscillating along the *c* axis, which is perpendicular to *a* and *b*. The complex Rabi frequency, describing an electric dipole transition between rotational states of a molecule, has opposite sign for the two enantiomers [165]. Therefore, the oscillation along the *c* axis has a phase shift of π for the two enantiomers (blue quarter circle for the first and purple quarter circles for the second enantiomer in Figure 12 b). Adding a third *c*-polarized $\pi/2$ pulse connecting $|g\rangle$ and $|e_c\rangle$, with a controlled phase relative to the first two pulses, it is possible to transfer the population of one enantiomer to the excited state and the population of the second enantiomer back to the ground state. This is indicated in Figure 12 c by green quarter circles and arrows. Finally, when traversing an electric deflector, the two enantiomers in the molecular beam will be spatially dispersed by the electrostatic deflector due to the different effective dipole moments of the two states they reside in. Enantiomeric pure samples are obtained by making use of skimmers properly positioned in the molecular beam and are thus available for applications, e.g., precision-spectroscopy experiments.

4.3. Nonadiabatic effects

The complex energy level structure of molecules in external fields provides a serious challenge for their theoretical description [98, 100, 166–169]. Especially for the general case of an asymmetric top a high density of states and low symmetry of the system [96] leads to many adiabatically avoided crossings. Studies of the nonadiabaticity in the network of dense crossings is a challenging but intriguing problem. The investigation of the resulting nonadiabatic dynamics in the interaction of a molecule with a strong

electric field might be accessible through the electric deflector. In its inhomogeneous strong electric field the molecules are exploring the energy landscape of their pendular states. The passing speed of the system at an avoided crossing, and, therefore, its adiabaticity is dependent on the rate of change of the electric field strength. By controlling the rate of change of the applied voltages for a defined electrode geometry, it is possible to control the speed of passing through the avoided crossings. This can be achieved through high-voltage switching using experimentally well-defined rise and fall times. Moreover, the deflector can be used as a quantum state detector. In a first experiment the quantum state properties and populations in the molecular beam are characterized with the electric deflector. In a second experiment the molecules are exposed to a time-dependent electric field before they enter the deflector. The rise time of the electric field is chosen such that the molecules pass an avoided crossing non-adiabatically. The fall time of the electric field should ideally be slow enough to recross it adiabatically. Such a switching procedure ensures that the molecules only traverse the avoided crossing non-adiabatically once. The modified quantum-state distribution is again characterized by the electric deflector. Multiple field gradients can be explored to increase the obtained amount of information on the avoided crossing. Comparison with the quantum-state distribution without switching the electric field yields the population transfer distribution through the avoided crossing and allows to unravel the physics of non adiabatic behaviour at individual and connected avoided crossings. For typical avoided crossings a rise time of the electric field on the order of 10^{18} V/(m s) (e.g., 1000 kV/cm in 100 ps) is required in order to become impulsive. This is about three orders of magnitude faster than possible with current technology, but the necessary technologies might become available in the future.

4.4. Cyclic deflectors

The quantum state resolution behind a deflecting device can be increased by changing the shape of the electrodes [102], extending it or by using several deflectors behind each other. Increasing the length of a single straight deflector will eventually result in the molecules crashing into its electrodes [120]. Alternatively a curved deflector electrode could be used. Assuming a favorable deflection of 3 mm after a 15 cm long deflector this would result in a radius of approximately 4 m for such a device, allowing for very strong quantum-state discrimination. We point out that the molecules are not actually trapped, since they are in hfs states and, therefore, are always attracted by the electrodes of the deflector. This has the consequence that such a setup is not a storage ring. Nevertheless, the molecules will traverse the device for a significant amount of time on metastable trajectories. For typical beam conditions as described in section 3, we estimate a number density of $10^4/\text{cm}^3$ in a very pure single-quantum-state sample after one round trip in such a device.

4.5. Merged-beam reactive scattering

Extending the ion-molecule reactions described in subsection 3.1, applications for crossed- and merged-beam reactive-scattering experiments with large molecules are envisioned, similar to current experiments with atoms and small molecules [170–

172]. Using curved deflector electrodes (see subsection 4.4), two velocity-matched beams of polar molecules can be merged in virtually any, lfs or hfs, single or small set of quantum states. Due to the low relative velocities, and the correspondingly small number of partial waves contributing to the reaction, possible scattering resonances [171, 173, 174] may become visible even in the reactions of complex molecules.

In addition a movable skimmer behind the deflector could serve as a selector for molecules in specific quantum states. This results in a molecular beam of selected molecular species in selected quantum-states, which can be exploited for reactive scattering experiments. Furthermore, a deflector in the outgoing beam could even disperse and analyse the product states and species distributions. Moreover, as described in subsection 3.4, the deflector can be used to create strongly aligned and oriented samples, which allow for the investigation of steric effects in these chemical reactions [175, 176].

4.6. Matrix deposition experiments

As a further application, one could envision to exploit the deflector for the deposition of selected nuclear-spin isomers, structural isomers, enantiomers, or even specific molecular clusters in a cryogenic rare gas matrix [177, 178]. Due to the extended observation periods and the low temperatures in these matrices, such low-temperature storage would allow for precision molecular spectroscopy as well as the investigation of slow dynamic processes, similar to studies of nuclear-spin relaxation, for instance, of water [179, 180]. These experiments could be extended to investigations of structural isomerisation reactions or the bond-breaking and forming in specific clusters, providing novel insight into these basic yet complex chemical transformations.

5. Conclusions

Inhomogeneous electric fields provide means to control the motion of even complex molecules. Modern technologies and insight into these approaches, such as extreme supersonic expansions, strong, possibly switched, electric fields and a detailed quantitative understanding of the interaction of molecules with these strong fields has enabled the realisation of novel control experiments. Exploiting appropriately shaped and timed fields, these approaches allow for the separation of molecules based on their effective dipole moment, i. e., their internal state and, therefore, the creation of gas-phase samples of molecules in selected quantum states, isomers, and cluster sizes. We have described experiments that have purified beams of individual quantum states, isomers, and sizes, as well as a number of first applications of these well-defined samples in chemical reaction studies, further control experiments, and for ultrafast molecular imaging. In order to facilitate the application of the electric deflector in further laboratories and experiments, we provide an educational script to simulate the trajectories of molecules through an electric deflector apparatus. Further applications have been detailed, which we consider feasible with the current state of the art. They range from improved selectivity and the selection of considerably larger and more complex molecules, over studies of fundamental effects and symmetries, to opportunities for disentangling the chemical reaction kinetics and dynamics of large

and complex molecules.

Overall, the development of a detailed, microscopic, reductionist understanding of the structure-function relationship in the molecular sciences relies on the ability to produce clean samples of pure “molecules”, in the gas phase. Pushing these experiments into new regimes relies on further technological advances. Especially for the far-reaching goal of controlling very large biological “molecules”, like proteins or viruses, novel concepts to control these particles are required [63, 64]. Major advances in the field of time and structure resolving imaging methods [6] will also be necessary. We believe that the experiments described in this paper are an important step forward, but at the same time we realise that “there is plenty of room at the top” to bridge small-molecule physical chemistry with large-scale chemistry and (structural) biology.

Acknowledgements

The experiments described in this article in which we have been involved are the result of more than ten years of research by a large group of people. The efforts started at the Department of Molecular Physics (headed by Gerard Meijer) of the Fritz Haber Institute of the Max Planck Society in 2003. In 2010, my group moved to the Center for Free-Electron Laser Science at DESY and the University of Hamburg. We are greatly indebted to the technical, administrative, and scientific staff at these institutions, and we thank all of the students, postdocs, senior scientists, and our external collaborators that have been involved in this work, and without whom these experiments would not have been possible.

We wish to thank Frank Filsinger, Gerard Meijer, Jonas L. Hansen, Jochen Maurer, Jens H. Nielsen, Lotte Holmegaard, and Henrik Stapelfeldt for help with the measurements presented in Figure 5 and Joss Wiese for help with the measurements presented in Figure 7.

Besides DESY, this work has been supported by the Helmholtz Association “Initiative and Networking Fund”, the Max Planck Society, the *Deutsche Forschungsgemeinschaft* (DFG) through the priority program “SPP 1116: Interactions in ultracold atomic and molecular gases” (KU1527/1) and the excellence cluster “The Hamburg Center for Ultrafast Imaging – Structure, Dynamics and Control of Matter at the Atomic Scale” (CUI, DFG-EXC1074), and the European Research Council through the Consolidator Grant 614507-COMOTION.

References

- [1] J. Kraitchman, *Am. J. Phys.* **21**, 17 (1953).
- [2] D. W. Pratt, *Annual Review of Physical Chemistry* **49** (1), 481–530 (1998). <<http://physchem.annualreviews.org/cgi/content/abstract/49/1/481>>.
- [3] K. Wüthrich, *Angew. Chem. Int. Ed.* **42** (29), 3340–3363 (2003).
- [4] S. T. Shipman and B. H. Pate, in *Handbook of High-resolution Spectroscopy*, edited by M. Quack and F. Merkt (John Wiley & Sons, Ltd, Chichester, UK, 2011), Chap. 36, pp. 801–827.
- [5] C. Pérez, M. T. Muckle, D. P. Zaleski, N. a. Seifert, B. Temelso, G. C. Shields, Z. Kisiel, and B. H. Pate, *Science* **336** (6083), 897–901 (2012). <<http://www.ncbi.nlm.nih.gov/pubmed/22605772>>.
- [6] A. Barty, J. Küpper, and H. N. Chapman, *Annu. Rev. Phys. Chem.* **64** (1), 415–435 (2013). <<http://dx.doi.org/10.1146/annurev-physchem-032511-143708>>.
- [7] R. J. D. Miller, *Science* **343** (6175), 1108–1116 (2014).
- [8] C. Ratzer, J. Küpper, D. Spangenberg, and M. Schmitt, *Chem. Phys.* **283** (1), 153–169 (2002). <[http://dx.doi.org/10.1016/S0301-0104\(02\)00591-8](http://dx.doi.org/10.1016/S0301-0104(02)00591-8)>.
- [9] F. H. de Leeuw and A. Dymanus, *Chem. Phys. Lett.* **7** (2), 288–292 (1970).
- [10] M. Okrusch, R. Müller, and A. Hese, *J. Chem. Phys.* **110**, 10393–10402 (1999).

- [11] C. A. Royer, *Chem. Rev.* **106** (5), 1769–1784 (2006).
- [12] H. B. Mayes, L. J. Broadbelt, and G. T. Beckham, *J. Am. Chem. Soc.* **136** (3), 1008–1022 (2014).
- [13] A. J. Baldwin and L. E. Kay, *Nat. Chem. Biol.* **5** (11), 808–814 (2009).
- [14] D. G. Blackmond, *Cold Spring Harb. Perspect. Biol.* **2** (5), a002147 (2010).
- [15] A. Pross, *What is Life?: How chemistry becomes biology* (, , 2012).
- [16] R. D. Suenram and F. J. Lovas, *J. Am. Chem. Soc.* **102**, 7180–7184 (1980).
- [17] T. R. Rizzo, Y. D. Park, L. Peteanu, and D. H. Levy, *J. Chem. Phys.* **83**, 4819–4820 (1985).
- [18] G. Scoles, editor, *Atomic and molecular beam methods*, Vol. 1 & 2 (Oxford University Press, New York, NY, USA, 1988 & 1992).
- [19] J. B. Fenn, *Annu. Rev. Phys. Chem.* **47**, 1–41 (1996).
- [20] U. Erlekam, M. Frankowski, G. von Helden, and G. Meijer, *Phys. Chem. Chem. Phys.* **9**, 3786–3789 (2007).
- [21] S. Y. T. van de Meerakker, N. Vanhaecke, M. P. J. van der Loo, G. C. Groenenboom, and G. Meijer, *Phys. Rev. Lett.* **95** (1), 013003 (2005). <<http://link.aps.org/abstract/PRL/v95/e013003>>.
- [22] J. Küpper, F. Filsinger, and G. Meijer, *Faraday Disc.* **142**, 155–173 (2009).
- [23] S. Y. T. van de Meerakker, H. L. Bethlem, and G. Meijer, *Nat. Phys.* **4** (8), 595 (2008). <<http://dx.doi.org/10.1038/nphys1031>>.
- [24] M. Schnell and G. Meijer, *Angew. Chem. Int. Ed.* **48** (33), 6010–6031 (2009). <<http://dx.doi.org/10.1002/anie.200805503>>.
- [25] S. Y. T. van de Meerakker, H. L. Bethlem, N. Vanhaecke, and G. Meijer, *Chem. Rev.* **112** (9), 4828–4878 (2012). <<http://pubs.acs.org/doi/abs/10.1021/cr200349r>>.
- [26] H. L. Bethlem, G. Berden, F. M. H. Crompvoets, R. T. Jongma, A. J. A. van Roij, and G. Meijer, *Nature* **406**, 491–494 (2000). <<http://dx.doi.org/10.1038/35020030>>.
- [27] H. J. Loesch and A. Remscheid, *J. Chem. Phys.* **93**, 4779 (1990).
- [28] B. Friedrich and D. Herschbach, *Phys. Rev. Lett.* **74** (23), 4623–4626 (1995).
- [29] H. Stapelfeldt and T. Seideman, *Rev. Mod. Phys.* **75** (2), 543–557 (2003). <<http://link.aps.org/abstract/RMP/v75/p543>>.
- [30] L. Holmegaard, J. H. Nielsen, I. Nevo, H. Stapelfeldt, F. Filsinger, J. Küpper, and G. Meijer, *Phys. Rev. Lett.* **102**, 023001 (2009). <<http://dx.doi.org/10.1103/PhysRevLett.102.023001>>.
- [31] H. Kallmann and F. Reiche, *Z. Phys.* **6**, 352–375 (1921). <<http://dx.doi.org/10.1007/BF01327996>>.
- [32] W. Gerlach and O. Stern, *Z. Phys.* **9**, 349–352 (1922). <<http://dx.doi.org/10.1007/BF01326983>>.
- [33] E. Wrede, *Z. Phys.* **44** (4-5), 261–268 (1927). <<http://dx.doi.org/10.1007/BF01391193>>.
- [34] N. Vanhaecke, U. Meier, M. Andrist, B. H. Meier, and F. Merkt, *Phys. Rev. A* **75** (3), 031402(R) (2007).
- [35] E. Narevicius and M. G. Raizen, *Chem. Rev.* **112** (9), 4879–89 (2012). <<http://www.ncbi.nlm.nih.gov/pubmed/22827566>>.
- [36] O. Stern, *Z. Phys.* **39** (10-11), 751–763 (1926). <<http://dx.doi.org/10.1007/BF01451746>>.
- [37] I. I. Rabi, S. Millman, P. Kusch, and J. R. Zacharias, *Phys. Rev.* **55** (6), 526–535 (1939). <<http://journals.aps.org/pr/abstract/10.1103/PhysRev.55.526>>.
- [38] J. P. Gordon, H. J. Zeiger, and C. H. Townes, *Phys. Rev.* **95**, 282–284 (1954).
- [39] H. G. Bennewitz, W. Paul, and C. Schlier, *Z. Phys.* **141**, 6 (1955).
- [40] J. P. Gordon, *Phys. Rev.* **99**, 1253–1263 (1955).
- [41] J. P. Gordon, H. J. Zeiger, and C. H. Townes, *Phys. Rev.* **99**, 1264–1274 (1955).

- [42] J. van Veldhoven, J. Küpper, H. L. Bethlem, B. Sartakov, A. J. A. van Roij, and G. Meijer, *Eur. Phys. J. D* **31** (2), 337–349 (2004). <<http://dx.doi.org/10.1140/epjd/e2004-00160-9>>.
- [43] M. Hillenkamp, S. Keinan, and U. Even, *J. Chem. Phys.* **118** (19), 8699–8705 (2003). <<http://link.aip.org/link/?JCP/118/8699/1>>.
- [44] D. S. Jin and J. Ye, *Chem. Rev.* **112** (9), 4801–4802 (2012).
- [45] D. Auerbach, E. E. A. Bromberg, and L. Wharton, *J. Chem. Phys.* **45**, 2160 (1966).
- [46] F. Günther and K. Schügerl, *Z. Phys. Chem.* **NF 80**, 155 (1972).
- [47] F. Filsinger, U. Erlekam, G. von Helden, J. Küpper, and G. Meijer, *Phys. Rev. Lett.* **100**, 133003 (2008). <<http://dx.doi.org/10.1103/PhysRevLett.100.133003>>.
- [48] F. Filsinger, S. Putzke, H. Haak, G. Meijer, and J. Küpper, *Phys. Rev. A* **82**, 052513 (2010).
- [49] S. Putzke, F. Filsinger, H. Haak, J. Küpper, and G. Meijer, *Phys. Chem. Chem. Phys.* **13**, 18962 (2011).
- [50] H. L. Bethlem, A. J. A. van Roij, R. T. Jongma, and G. Meijer, *Phys. Rev. Lett.* **88** (13), 133003 (2002). <<http://doi.dx.org/10.1103/PhysRevLett.88.133003>>.
- [51] M. R. Tarbutt, H. L. Bethlem, J. J. Hudson, V. L. Ryabov, V. A. Ryzhov, B. E. Sauer, G. Meijer, and E. A. Hinds, *Phys. Rev. Lett.* **92** (17), 173002 (2004). <<http://dx.doi.org/10.1103/PhysRevLett.92.173002>>.
- [52] H. L. Bethlem, M. R. Tarbutt, J. Küpper, D. Carty, K. Wohlfart, E. A. Hinds, and G. Meijer, *J. Phys. B* **39** (16), R263–R291 (2006). <<http://dx.doi.org/10.1088/0953-4075/39/16/R01>>.
- [53] K. Wohlfart, F. Filsinger, F. Grätz, J. Küpper, and G. Meijer, *Phys. Rev. A* **78** (3), 033421 (2008).
- [54] K. Wohlfart, F. Grätz, F. Filsinger, H. Haak, G. Meijer, and J. Küpper, *Phys. Rev. A* **77**, 031404(R) (2008). <<http://dx.doi.org/10.1103/PhysRevA.77.031404>>.
- [55] F. Filsinger, G. Meijer, H. Stapelfeldt, H. Chapman, and J. Küpper, *Phys. Chem. Chem. Phys.* **13** (6), 2076–2087 (2011).
- [56] H. Odashima, S. Merz, K. Enomoto, M. Schnell, and G. Meijer, *Phys. Rev. Lett.* **104**, 253001 (2010).
- [57] H. Stapelfeldt, H. Sakai, E. Constant, and P. B. Corkum, *Phys. Rev. Lett.* **79**, 2787–2790 (1997). <<http://dx.doi.org/10.1103/PhysRevLett.79.2787>>.
- [58] B. S. Zhao, H. S. Chung, K. Cho, S. H. Lee, S. Hwang, J. Yu, Y. H. Ahn, J. Y. Sohn, D. S. Kim, W. K. Kang, and D. S. Chung, *Phys. Rev. Lett.* **85** (13), 2705–2708 (2000).
- [59] R. Fulton, A. I. Bishop, M. N. Shneider, and P. F. Barker, *Nat. Phys.* **2**, 465–468 (2006).
- [60] A. Ashkin, *Phys. Rev. Lett.* **24** (4), 156–159 (1970). <<http://link.aps.org/doi/10.1103/PhysRevLett.24.156>>.
- [61] P. Lebedew, *Ann. Phys.* **311** (11), 433–458 (1901). <<http://doi.wiley.com/10.1002/andp.19013111102>>.
- [62] F. Ehrenhaft, *Ann. Phys.* **361** (10), 81–132 (1918). <<http://doi.wiley.com/10.1002/andp.19183611002>>.
- [63] N. Eckerskorn, L. Li, R. A. Kirian, J. Küpper, D. P. DePonte, W. Krolikowski, W. M. Lee, H. N. Chapman, and A. V. Rode, *Opt. Exp.* **21** (25), 30492–30499 (2013).
- [64] Controlling the Motion of Complex Molecules and Particles (COMOTION) 2015. <<http://www.comotion.info>>.
- [65] T. R. Rizzo, Y. D. Park, L. A. Peteanu, and D. H. Levy, *J. Chem. Phys.* **84**, 2534–2541 (1986).
- [66] M. S. de Vries and P. Hobza, *Annu. Rev. Phys. Chem.* **58**, 585–612 (2007).
- [67] J. L. Neill, K. O. Douglass, B. H. Pate, and D. W. Pratt, *Phys. Chem. Chem. Phys.* **13** (16), 7253–7262 (2011).
- [68] J. Watson and F. Crick, *Nature* **171** (4356), 737–738 (1953). <<http://dx.doi.org/>>

- 10.1038/171737a0>.
- [69] K. Hedberg, L. Hedberg, D. S. Bethune, C. A. Brown, H. C. Dorn, R. D. Johnson, and M. de Vries, *Science* **254** (5030), 410–412 (1991). <<http://www.sciencemag.org/cgi/content/abstract/254/5030/410>>.
 - [70] J. C. Williamson, J. M. Cao, H. Ihee, H. Frey, and A. H. Zewail, *Nature* **386** (6621), 159–162 (1997).
 - [71] G. Sciaini and R. J. D. Miller, *Rep. Prog. Phys.* **74** (9), 096101 (2011). <<http://iopscience.iop.org/0034-4885/74/9/096101/>>.
 - [72] R. Neutze, R. Wouts, D. van der Spoel, E. Weckert, and J. Hajdu, *Nature* **406** (6797), 752–757 (2000). <<http://dx.doi.org/10.1038/35021099>>.
 - [73] C. J. Hensley, J. Yang, and M. Centurion, *Phys. Rev. Lett.* **109**, 133202 (2012).
 - [74] J. Küpper, S. Stern, L. Holmegaard, F. Filsinger, A. Rouzée, A. Rudenko, P. Johnsson, A. V. Martin, M. Adolph, A. Aquila, S. Bajt, A. Barty, *et al.*, *Phys. Rev. Lett.* **112**, 083002 (2014).
 - [75] K. L. Reid, *Molecular Physics* **3**, 131–147 (2012).
 - [76] C. Z. Bisgaard, O. J. Clarkin, G. Wu, A. M. D. Lee, O. Gefner, C. C. Hayden, and A. Stolow, *Science* **323** (5920), 1464–1468 (2009).
 - [77] L. Holmegaard, J. L. Hansen, L. Kalhøj, S. L. Kragh, H. Stapelfeldt, F. Filsinger, J. Küpper, G. Meijer, D. Dimitrovski, M. Abu-samha, C. P. J. Martiny, and L. B. Madsen, *Nat. Phys.* **6**, 428 (2010).
 - [78] H. Akagi, T. Otobe, A. Staudte, A. Shiner, F. Turner, R. Dörner, D. Villeneuve, and P. Corkum, *Science* **325** (5946), 1364–1367 (2009).
 - [79] J. Hansen, H. Stapelfeldt, D. Dimitrovski, M. Abu-Samha, C. Martiny, and L. Madsen, *Phys. Rev. Lett.* **106** (7), 073001 (2011). <<http://prl.aps.org/abstract/PRL/v106/i7/e073001>>.
 - [80] J. Maurer, D. Dimitrovski, L. Christensen, L. B. Madsen, and H. Stapelfeldt, *Phys. Rev. Lett.* **109**, 123001 (2012). <<http://link.aps.org/doi/10.1103/PhysRevLett.109.123001>>.
 - [81] T. Zuo, A. D. Bandrauk, and P. B. Corkum, *Chem. Phys. Lett.* **259** (3-4), 313–320 (1996).
 - [82] C. I. Blaga, J. Xu, A. D. DiChiara, E. Sistrunk, K. Zhang, P. Agostini, T. A. Miller, L. F. DiMauro, and C. D. Lin, *Nature* **483** (7388), 194–197 (2012).
 - [83] J. Itatani, J. Levesque, D. Zeidler, H. Niikura, H. Pépin, J. C. Kieffer, P. B. Corkum, and D. M. Villeneuve, *Nature* **432**, 867–871 (2004).
 - [84] H. J. Wörner, J. B. Bertrand, D. V. Kartashov, P. B. Corkum, and D. M. Villeneuve, *Nature* **466** (7306), 604–607 (2010).
 - [85] A. Landers, T. Weber, I. Ali, A. Cassimi, M. Hattass, O. Jagutzki, A. Nauert, T. Osipov, A. Staudte, M. H. Prior, H. Schmidt-Böcking, C. L. Cocke, *et al.*, *Phys. Rev. Lett.* **87** (1), 013002 (2001). <<http://prola.aps.org/abstract/PRL/v87/i1/e013002>>.
 - [86] F. Krasniqi, B. Najjari, L. Strüder, D. Rolles, A. Voitkiv, and J. Ullrich, *Phys. Rev. A* **81**, 033411 (2010).
 - [87] R. Boll, D. Anielski, C. Bostedt, J. D. Bozek, L. Christensen, R. Coffee, S. De, P. Decleva, S. W. Epp, B. Erk, L. Foucar, F. Krasniqi, *et al.*, *Phys. Rev. A* **88**, 061402(R) (2013).
 - [88] Y. T. Lee, *Science* **236** (4803), 793–798 (1987).
 - [89] A. H. Zewail, *J. Phys. Chem. A* **104** (24), 5660–5694 (2000).
 - [90] W. S. Warren, H. Rabitz, and M. Dahleh, *Science* **259**, 1581–1589 (1993). <<http://www.jstor.org/stable/2880660>>.
 - [91] A. Assion, T. Baumert, M. Bergt, T. Brixner, B. Kiefer, V. Seyfried, M. Strehle, and G. Gerber, *Science* **282**, 919–922 (1998). <<http://dx.doi.org/10.1126/science.282.5390.919>>.

- [92] T. Wang, J. Chen, T. Yang, C. Xiao, Z. Sun, L. Huang, D. Dai, X. Yang, and D. H. Zhang, *Science* **342** (6165), 1499–1502 (2013).
- [93] S. N. Vogels, J. Onvlee, A. von Zastrow, G. C. Groenenboom, A. van der Avoird, and S. Y. T. Meerakker, *Phys. Rev. Lett.* **113** (26), 263202 (2014).
- [94] H. Ihee, V. Lobastov, U. Gomez, B. Goodson, R. Srinivasan, C. Ruan, and A. H. Zewail, *Science* **291** (5503), 458–462 (2001).
- [95] W. Gordy and R. L. Cook, *Microwave Molecular Spectra*, 3rd ed. (John Wiley & Sons, New York, NY, USA, 1984).
- [96] Y. P. Chang, F. Filsinger, B. Sartakov, and J. Küpper, *Comp. Phys. Comm.* **185**, 339–49 (2014). <<http://www.sciencedirect.com/science/article/pii/S0010465513003019>>.
- [97] K. Wohlfart, M. Schnell, J. U. Grabow, and J. Küpper, *J. Mol. Spec.* **247** (1), 119–121 (2008). <<http://dx.doi.org/10.1016/j.jms.2007.10.006>>.
- [98] M. Abd El Rahim, R. Antoine, M. Broyer, D. Rayane, and P. Dugourd, *J. Phys. Chem. A* **109** (38), 8507–14 (2005). <<http://www.ncbi.nlm.nih.gov/pubmed/16834247>>.
- [99] N. F. Ramsey, *Molecular Beams* The International Series of Monographs on Physics (Oxford University Press, London, GB, 1956; reprinted in *Oxford Classic Texts in the Physical Sciences* (2005)), reprinted in *Oxford Classic Texts in the Physical Sciences* (2005).
- [100] F. Filsinger, J. Küpper, G. Meijer, L. Holmegaard, J. H. Nielsen, I. Nevo, J. L. Hansen, and H. Stapelfeldt, *J. Chem. Phys.* **131**, 064309 (2009). <<http://scitation.aip.org/content/aip/journal/jcp/131/6/10.1063/1.3194287>>.
- [101] J. G. Kalnins, G. Lambertson, and H. Gould, *Rev. Sci. Instrum.* **73**, 2557–2565 (2002). <<http://scitation.aip.org/content/aip/journal/rsi/73/7/10.1063/1.1485778>>.
- [102] A. J. de Nijs and H. L. Bethlem, *Phys. Chem. Chem. Phys.* **13** (42), 19052–8 (2011). <<http://www.ncbi.nlm.nih.gov/pubmed/21979152>>.
- [103] T. M. Miller and B. Bederson, *Adv. Atom. Mol. Opt. Phys.* **25**, 37–60 (1988).
- [104] R. Schäfer, S. Schlecht, J. Woenckhaus, and J. Becker, *Phys. Rev. Lett.* **76** (3), 471–474 (1996). <http://prl.aps.org/abstract/PRL/v76/i3/p471_1>.
- [105] W. A. de Heer and V. V. Kresin, arXiv p. 0901.4810 (2009). <<http://de.arxiv.org/abs/0901.4810>>, Article prepared for the Handbook of Nanophysics, ed. by Klaus D. Sattler, to be published by Taylor&Francis/CRC Press.
- [106] S. Trippel, T. Mullins, N. L. M. Müller, J. S. Kienitz, K. Długołęcki, and J. Küpper, *Mol. Phys.* **111**, 1738 (2013).
- [107] A. J. de Nijs, W. Ubachs, and H. L. Bethlem, *J. Mol. Spec.* **300**, 79–85 (2014).
- [108] H. Nishimura, G. Lambertson, J. G. Kalnins, and H. Gould, *Rev. Sci. Instrum.* **74** (7), 3271–2378 (2003). <<http://doi.dx.org/10.1063/1.1578159>>.
- [109] S. Putzke, Alternating-gradient focusing of large neutral molecules, Dissertation, Freie Universität, Berlin 2012.
- [110] S. Trippel, Y. P. Chang, S. Stern, T. Mullins, L. Holmegaard, and J. Küpper, *Phys. Rev. A* **86**, 033202 (2012). <<http://pra.aps.org/abstract/PRA/v86/i3/e033202>>.
- [111] K. Luria, W. Christen, and U. Even, *J. Phys. Chem. A* **115** (25), 7362–7367 (2011).
- [112] R. Escibano, B. Mate, F. Ortigoso, and J. Ortigoso, *Phys. Rev. A* **62** (2), 023407 (2000).
- [113] T. E. Wall, S. K. Tokunaga, E. a. Hinds, and M. R. Tarbutt, *Phys. Rev. A* **81** (3), 033414 (2010). <<http://link.aps.org/doi/10.1103/PhysRevA.81.033414>>.
- [114] M. Kirste, B. G. Sartakov, M. Schnell, and G. Meijer, *Phys. Rev. A* **79**, 051401(R) (2009). <<http://dx.doi.org/10.1103/PhysRevA.79.051401>>.
- [115] J. van Veldhoven, R. T. Jongma, B. Sartakov, W. A. Bongers, and G. Meijer, *Phys. Rev. A* **66** (3), 32501 (2002).
- [116] F. Filsinger, Manipulation of large neutral molecules with electric fields, Ph.D. thesis,

Radboud Universiteit, Nijmegen, The Netherlands 2010.

- [117] J. H. Nielsen, P. Simesen, C. Z. Bisgaard, H. Stapelfeldt, F. Filsinger, B. Friedrich, G. Meijer, and J. Küpper, *Phys. Chem. Chem. Phys.* **13**, 18971–18975 (2011).
- [118] S. Trippel, T. Mullins, N. L. M. Müller, J. S. Kienitz, J. J. Omiste, H. Stapelfeldt, R. González-Férez, and J. Küpper, *Phys. Rev. A* **89**, 051401(R) (2014).
- [119] D. A. Horke, Y. P. Chang, K. Długołęcki, and J. Küpper, *Angew. Chem. Int. Ed.* **53**, 11965–11968 (2014). <<http://onlinelibrary.wiley.com/doi/10.1002/anie.201405986/abstract>>.
- [120] F. Filsinger, J. Küpper, G. Meijer, J. L. Hansen, J. Maurer, J. H. Nielsen, L. Holmegaard, and H. Stapelfeldt, *Angew. Chem. Int. Ed.* **48**, 6900–6902 (2009). <<http://onlinelibrary.wiley.com/doi/10.1002/anie.200902650/abstract>>.
- [121] T. Kierspel, D. A. Horke, Y. P. Chang, and J. Küpper, *Chem. Phys. Lett.* **591**, 130–132 (2014). <<http://www.sciencedirect.com/science/article/pii/S0009261413014000>>.
- [122] Y. P. Chang, K. Długołęcki, J. Küpper, D. Rösch, D. Wild, and S. Willitsch, *Science* **342** (6154), 98–101 (2013). <<http://dx.doi.org/10.1126/science.1242271>>.
- [123] G. von Helden, T. Wyttenbach, and M. T. Bowers, *Science* **267**, 1483–1485 (1995).
- [124] M. Jarrold, *Phys. Chem. Chem. Phys.* **9**, 1659–1671 (2007).
- [125] G. Papadopoulos, A. Svendsen, O. V. Boyarkin, and T. R. Rizzo, *Faraday Disc.* **150**, 243–255 (2011). <<http://dx.doi.org/10.1039/C0FD00004C>>.
- [126] A. B. Kanu, P. Dwivedi, M. Tam, L. Matz, and H. H. Hill, *J. Mass. Spectrom.* **43** (1), 1–22 (2008).
- [127] S. T. Park, S. K. Kim, and M. S. Kim, *Nature* **415**, 306 (2002). <<http://www.nature.com/nature/journal/v415/n6869/abs/415306a.html>>.
- [128] M. H. Kim, L. Shen, H. Tao, T. J. Martinez, and A. G. Suits, *Science* **315**, 1561 (2007). <<http://www.sciencemag.org/content/315/5818/1561>>.
- [129] B. C. Dian, J. R. Clarkson, and T. S. Zwier, *Science* **303** (5661), 1169–1173 (2004). <<http://www.sciencemag.org/cgi/content/abstract/303/5661/1169>>.
- [130] B. C. Dian, A. Longarte, and T. S. Zwier, *Science* **296** (5577), 2369–2373 (2002). <<http://www.sciencemag.org/cgi/content/abstract/296/5577/2369>>.
- [131] K. Wohlfart, Alternating-gradient focusing and deceleration of large molecules, Dissertation, Free University, Berlin, Germany 2008. <http://www.diss.fu-berlin.de/diss/receive/FUDISS_thesis_000000004336>.
- [132] D. A. Horke, S. Trippel, Y. P. Chang, S. Stern, T. Mullins, T. Kierspel, and J. Küpper, *J. Vis. Exp.* p. e51137 (2014). <<http://www.jove.com/video/51137/spatial-separation-of-molecular-conformers-and-clusters>>.
- [133] S. Trippel, T. Mullins, N. L. M. Müller, J. S. Kienitz, R. González-Férez, and J. Küpper, *Phys. Rev. Lett.* **114**, 103003 (2015).
- [134] D. Rösch, S. Willitsch, Y. P. Chang, and J. Küpper, *J. Chem. Phys.* **140** (12), 124202 (2014). <<http://dx.doi.org/10.1063/1.4869100>>.
- [135] S. Willitsch, *Int. Rev. Phys. Chem.* **31**, 175 (2012). <<http://www.tandfonline.com/doi/abs/10.1080/0144235X.2012.667221>>.
- [136] X. Tong, A. H. Winney, and S. Willitsch, *Phys. Rev. Lett.* **105**, 143001 (2010). <<http://link.aps.org/doi/10.1103/PhysRevLett.105.143001>>.
- [137] J. R. R. Verlet, *Chem. Soc. Rev.* **37**, 505–517 (2008).
- [138] A. Fujii and K. Mizuse, *Int. Rev. Phys. Chem.* **32** (2), 266–307 (2013).
- [139] U. Buck and H. Meyer, *Phys. Rev. Lett.* **52** (2), 109–112 (1984). <<http://link.aps.org/doi/10.1103/PhysRevLett.52.109>>.
- [140] A. Goerke, M. Feser, H. Palm, C. Schulz, and I. Hertel, *Z. Phys. D* **19** (4), 137–139 (1991).
- [141] U. Buck and F. Huiskens, *Chem. Rev.* **100** (11), 3863–3890 (2000). <<http://dx.doi.org/10.1021/cr990054v>>.

- [142] S. Putzke, F. Filsinger, J. Küpper, and G. Meijer, *J. Chem. Phys.* **137** (10), 104310 (2012). <<http://link.aip.org/link/?JCPSA6/137/104310/1>>.
- [143] C. Kang, T. M. Korter, and D. W. Pratt, *J. Chem. Phys.* **122** (17), 174301 (2005). <<http://link.aip.org/link/?JCP/122/174301/1>>.
- [144] H. G. Bennewitz and W. Paul, *Z. Phys.* **139**, 489 (1954). <<http://dx.doi.org/10.1007/BF01374557>>.
- [145] J. Reuss, in *Atomic and molecular beam methods*, edited by G. Scoles, Vol. 1, Chap. 11 (Oxford University Press, New York, NY, USA, 1988), pp. 276–292.
- [146] H. L. Bethlem, G. Berden, and G. Meijer, *Phys. Rev. Lett.* **83**, 1558–1561 (1999). <<http://link.aps.org/abstract/PRL/v83/p1558>>.
- [147] M. Brouard, D. H. Parker, and S. Y. T. van de Meerakker, *Chem. Soc. Rev.* (2014). <<http://dx.doi.org/10.1039/c4cs00150h>>.
- [148] H. G. Bennewitz, K. H. Kramer, J. P. Toennies, and W. Paul, *Z. Phys.* **177** (1), 84 (1964).
- [149] P. R. Brooks and E. M. Jones, *J. Chem. Phys.* **45** (9), 3449 (1966).
- [150] R. J. Beuhler, R. B. Bernstein, and K. H. Kramer, *J. Am. Chem. Soc.* **88** (22), 5331 (1966).
- [151] V. Kumarappan, C. Z. Bisgaard, S. S. Viftrup, L. Holmegaard, and H. Stapelfeldt, *J. Chem. Phys.* **125** (19), 194309 (2006).
- [152] I. Nevo, L. Holmegaard, J. H. Nielsen, J. L. Hansen, H. Stapelfeldt, F. Filsinger, G. Meijer, and J. Küpper, *Phys. Chem. Chem. Phys.* **11**, 9912–9918 (2009).
- [153] D. Rolles, R. Boll, M. Adolph, A. Aquila, C. Bostedt, J. Bozek, H. Chapman, R. Coffee, N. Coppola, P. Decleva, T. Delmas, S. Epp, *et al.*, *J. Phys. B* **47** (12), 124035 (2014).
- [154] S. Stern, L. Holmegaard, F. Filsinger, A. Rouzee, A. Rudenko, P. Johnsson, A. V. Martin, A. Barty, C. Bostedt, J. Bozek, R. Coffee, S. Epp, *et al.*, *Faraday Disc.* **171**, 393 (2014).
- [155] F. Calvo and P. Dugourd, *Biophys. J.* **95** (1), 18–32 (2008).
- [156] A. Abrikossov, Computer simulation of Lysozyme in vacuum under the effect of an electric field, Examensarbete, Biomedical Center, Uppsala 2011. <<http://www.diva-portal.org/smash/get/diva2:410123/FULLTEXT01.pdf>>.
- [157] T. D. Lee and C. N. Yang, *Phys. Rev.* **104** (1), 254–258 (1956). <<http://dx.doi.org/10.1103/PhysRev.104.254>>.
- [158] C. S. Wu, E. Ambler, R. W. Hayward, D. D. Hoppes, and R. P. Hudson, *Phys. Rev.* **105** (4), 1413–1415 (1957). <<http://dx.doi.org/10.1103/PhysRev.105.1413>>.
- [159] B. Darquié, C. Stoeffler, A. Shelkovnikov, C. Daussy, A. Amy-Klein, C. Chardonnet, S. Zrig, L. Guy, J. Crassous, P. Soulard, P. Asselin, T. R. Huet, *et al.*, *Chirality* **22** (10), 870–884 (2010). <<http://doi.wiley.com/10.1002/chir.20911>>.
- [160] M. Quack, in *Quantum Systems in Chemistry and Physics*, edited by K. Nishikawa, J. Maruani, E. J. Brändas, G. Delgado-Barrio, and P. Piecuch, Chap. 3 (Springer Netherlands, Dordrecht, 2012), pp. 47–76. <<http://link.springer.com/10.1007/978-94-007-5297-9>>.
- [161] M. Quack, *Angew. Chem. Int. Ed.* **41**, 4618–4630 (2002).
- [162] C. Daussy, T. Marrel, A. Amy-Klein, C. T. Nguyen, C. J. Bordé, and C. Chardonnet, *Phys. Rev. Lett.* **83**, 1554–1557 (1999).
- [163] C. Medcraft, R. Wolf, and M. Schnell, *Angew. Chem. Int. Ed.* **53**, 11656 (2014).
- [164] D. Patterson, M. Schnell, and J. M. Doyle, *Nature* **497** (7450), 475–477 (2013).
- [165] A. Jacob and K. Hornberger, *J. Chem. Phys.* **137** (4), 044313 (2012). <<http://scitation.aip.org/content/aip/journal/jcp/137/4/10.1063/1.4738753>>.
- [166] M. Härtelt and B. Friedrich, *J. Chem. Phys.* **128** (22), 224313 (2008).
- [167] J. J. Omiste, M. Gaerttner, P. Schmelcher, R. González-Férez, L. Holmegaard, J. H. Nielsen, H. Stapelfeldt, and J. Küpper, *Phys. Chem. Chem. Phys.* **13** (42), 18815–

- 18824 (2011).
- [168] J. H. Nielsen, H. Stapelfeldt, J. Küpper, B. Friedrich, J. J. Omiste, and R. González-Férez, *Phys. Rev. Lett.* **108** (19), 193001 (2012). <<http://prl.aps.org/abstract/PRL/v108/i19/e193001>>.
 - [169] J. L. Hansen, J. J. Omiste Romero, J. H. Nielsen, D. Pentlehner, J. Küpper, R. González-Férez, and H. Stapelfeldt, *J. Chem. Phys.* **139**, 234313 (2013).
 - [170] M. Kirste, X. Wang, H. C. Schewe, G. Meijer, K. Liu, A. van der Avoird, L. M. C. Janssen, K. B. Gubbels, G. C. Groenenboom, and S. Y. T. van de Meerakker, *Science* **338** (6110), 1060–1063 (2012). <<http://www.sciencemag.org/cgi/doi/10.1126/science.1229549>>.
 - [171] A. B. Henson, S. Gersten, Y. Shagam, J. Narevicius, and E. Narevicius, *Science* **338** (6104), 234–238 (2012). <<http://www.sciencemag.org/cgi/doi/10.1126/science.1229141>>.
 - [172] J. Jankunas, B. Bertsche, and A. Osterwalder, *J. Phys. Chem. A* **118** (22), 3875–3879 (2014).
 - [173] X. Yang, *Annu. Rev. Phys. Chem.* **58** (1), 433–459 (2007). <<http://dx.doi.org/10.1146/annurev.physchem.58.032806.104632>>.
 - [174] S. Chefdeville, Y. Kalugina, S. Y. T. van de Meerakker, C. Naulin, F. Lique, and M. Costes, *Science* **341** (6150), 1094–1096 (2013). <<http://www.sciencemag.org/cgi/doi/10.1126/science.1241395>>.
 - [175] P. R. Brooks, *Science* **193** (4247), 11 (1976).
 - [176] M. H. G. de Miranda, A. Chotia, B. Neyenhuis, D. Wang, G. Quémener, S. Ospelkaus, J. L. Bohn, J. Ye, and D. S. Jin, *Nature Physics* **7**, 502–507 (2011). <<http://www.nature.com/nphys/journal/vaop/ncurrent/full/nphys1939.html>>.
 - [177] E. Whittle, D. A. Dows, and G. C. Pimentel, *J. Chem. Phys.* **22** (11), 1943–1943 (1954). <<http://dx.doi.org/10.1063/1.1739957>>.
 - [178] V. E. Bondybey, A. M. Smith, and J. Agreiter, *Chem. Rev.* **96** (6), 2113–2134 (1996).
 - [179] P. A. Turgeon, P. Ayotte, E. Lisitsin, Y. Meir, T. Kravchuk, and G. Alexandrowicz, *Phys. Rev. A* **86** (6), 062710 (2012). <<http://link.aps.org/doi/10.1103/PhysRevA.86.062710>>.
 - [180] R. Sliter, M. Gish, and A. F. Vilesov, *J. Phys. Chem. A* **115** (34), 9682–9688 (2011). <<http://dx.doi.org/10.1021/jp201125k>>.